مركز الأكاديمية للنشر
ACADEMY Publishing Center

RESD

Renewable Energy and Sustainable Development Journal

- ISSN 2356-8569

Volume 9
Issue 1
June 2023

Academy Publishing Center
Journal of Renewable Energy and Sustainable Development (RESD)

ACADEMY Publishing Center

RESD

Volume 9, Issue 1, June 2023
p-ISSN: 2356-8518 Print Version
e-ISSN: 2356-8569 Online Version

http://apc.aast.edu

Arab Academy for Science, Technology, and Maritime Transport, AASTMT Abu Kir Campus, Alexandria, EGYPT
P.O. Box: Miami 1029
Tel: (+203) 5622366/88 – EXT 1069 and (+203) 5611818
Fax: (+203) 5611818
Web Site: http://apc.aast.edu

RESD Journal of Renewable Energy and Sustainable Development

Renewable Energy and Sustainable Development (RESD) is a biannual international peer-reviewed journal, which presents a global forum for dissemination of research articles, case studies and reviews focusing on all aspects of renewable energy and its role in sustainable development. The topics of focal interest to RESD include, but are not limited to, all aspects of wind energy, wave/tidal energy, solar energy, as well as energy from biomass and biofuel. The integration of renewable energy technologies in electrical power networks and smart grids is another topic of interest to RESD. Experimental, computational and theoretical studies are all welcomed to RESD.

Sustainable development is a multidisciplinary advancing to the center of energy research with the declaration of UN millennium development goals for the first time in 2000, and continued to constitute a challenge in energy technologies in the past decade. RESD is mainly interested in case studies of sustainable development and its relation to transition economies in the Middle East, Africa, Asia and Oceania.

RESD has an outstanding editorial board of eminent scientists, researchers and engineers who contribute and enrich the journal with their vast experience in different fields of interest to the journal. The journal is open-access with a liberal Creative Commons Attribution-Non Commercial-4.0 International License. Which preserves the copyrights of published materials to the authors and protects it from unauthorized commercial use or derivation. The journal is financially supported by Arab Academy for Science, Technology and Maritime Transporting in order to maintain quality open-access source of research papers on renewable energy and sustainable development.

Editorial Committee

Advisory Board

Administrative Board

Contents

Journal of Renewable Energy and Sustainable Development (RESD) Volume 9, Issue 1, June 2023 - ISSN 2356-8569
http://dx.doi.org/10.21622/RESD.2023.09.1.001

Received on, 09 January 2023 Accepted on, 06 February 2023 Published on, 16 February 2023

Non-Uniform Dust Distribution Effect On Photovoltaic Panel Performance

Saman S. Jaafar[1a], Hiwa A. Maarof[1b], Renas T. Salh [1c], Hoshang Sahib[1d] and Yousif H. Azeez[1e]

[1]Physics department, College of Science, University of Halabja, Halabja, KRG-Iraq

[a]saman.jaafar@uoh.edu.iq, [b]Hiwa.Maroof@uoh.edu.iq, [c] renas.salh@uoh.edu.iq, [d]hoshang.sahib@uoh.edu.iq

[e]yousif.husain@uoh.ed.iq

ABSTRACT

A novel experimental method for power efficiency loss is presented in this paper. It is used to quantitatively determine the impact of dust deposition on the PV power generation panel. To determine the selection range of unknown parameters in the experiment process, a photovoltaic panel with five collected dust samples (Toner (C), Soil, Cement (CaO, SiO4), Gypsum (Ca2SO4.2H2O), and Sand (AL2O3, SiO4)) is designed. According to experimental results, the extinction coefficient for the five pollutants are recorded. Eventually, the impact of dusts on the results is proved by repeating in two continuous days of same conditions. The results show that the proposed process has a high effect on the reduction of output power (62% to 96%), decrease of irradiance (34% to 93%) and increase of output power due to increase of tilt angle as a doubling of power except toner. The experimental and calculated results are in agreement. The results show that non-uniform distribution of dust deposit pollutants on the photovoltaic panel significantly reduces the power output.

Index-words: *Dust deposition, Dust accumulation, Power reduction, Solar PV performance, Extinction coefficient.*

I. INTRODUCTION

With the industrial revolution and the increase in energy consumption, concerns about the environment and global warming have been raised (Mahmood, Jaafar, and Mustafa 2022). Recent worldwide efforts to improve energy security and reduce climate change have necessitated a fundamental shift in the way solar energy is handled [2]. Since photovoltaic (PV) phenomena were studied and solar cells were being made, countries have been using and relying on solar panels and modules for their electrical energy needs. The two prominent problems of PV are concerned with the environmental issues and energy that restricts the continuous development of economy and society. Installation of the solar panel depends on sseveral uncontrollable factors, and dust deposition on the surface of the PV is an important reason to decrease the power. Dust accumulation on the PV can scatter, reflect, and absorb the light, that will seriously drop the transmission of light and reduce the power (Fan et al. 2021). Furthermore, the variety of environmental factors decreased the efficiency of the PV by more than 30% (Memiche et al. 2020). The chemical decomposition, density, and size of dust particles are the reason behind decreasing the power (Mostefaoui et al. 2018) (Said et al. 2018). The design of dust cleaning on the surface of solar cells is highly recommended to increase the PV output power (Parrott et al. 2018). Dust accumulation of (10 g/m^2) decreases the performance of the PV by 34% (Chen et al. 2019), based on Salimi et al. (2020). The adhesion of dust particles is proportionally related to the reduction of the output power of PV (Kawamoto and Guo 2018). There are growing appeals for cleaning steps that are more useful to raise the performance of a dusty panel (Lorenz et al. 2019). Also, the industrial activities lead to deposit of different kinds of dust particles on the PV, which drops the electrical efficiency from 29% to 64% based on the types of deposited dust (Andrea, Pogrebnaya, and Kichonge 2019). The deposition of dust on the PV's surface will increase directly with the density and the size of particles, but it changes inversely with the diaphaneity of the particles (Xingcai and Kun 2018). Recently, theoretical developments have revealed that dust accumulation drops the PV's power by 29, 31, and 50% (Benghanem et al. 2018; Mostefaoui et al. 2018; Mussard and Amara 2018). Jaszczur (2018) stated that efficiency is reduced by 2.1% when 300mg of dust particles are deposited on each square meter. PV power is reduced directly with particles' densities; meanwhile, it has been changed based on the tilt angle of the PV. The tilt angle of 0° to 45° reduces performance by 37.6% to 10.9%, respectively (Hachicha, Al-sawafta, and Said 2019).

A suggested way to weaken the adhesion of dust on the glass surface of the PV is to use hydrophobic coating when, for tilt angles of 30° and 60°, the power reduction is 44.4% and 11.2%, respectively (Zhang et al. 2019). During dust storms, for angles of 0° to 45° tilt angle, the power efficiency of PV drops from 58.2% to 20.7% (Khodakaram-Tafti and Yaghoubi 2020) (Hachicha et al. 2019). The dirty solar panel has power production of 10% lower than the clean one. The different dust samples have been tested and it was revealed that they have reduced the performance

http://dx.doi.org/10.21622/RESD.2023.09.1.001

of the PV from 5% to 30% (Chaichan and Kazem 2020). The main adhesion forces between the dust particles and the PV surface are studied such as:

Capillary, Van der Waal, electrostatic and gravitational forces (Isaifan et al. 2019). Wang et al. (2018) showed that the coated PV with Fluorine super-hydrophobic film has less effect than the silicon super-hydrophobic film. The rainy weather can be mentioned as an excellent natural cleaner of dust on the PV (Panels 2020) (Al-Housani and Bicer 2019). A common strategy used to study the influence of dust deposition on the solar panel surface is to take a period of sandstorm going to deposit more thickness of dust particles and it leads to reducing the transmission of light (Mostefaoui et al. 2018). For decades, one of the most popular ideas for maintaining the highest performance in PV is the idea that the accumulated dust must be removed from its surface. The most detailed review of research has been done from 2012-2015, which shows the effects of dust accumulation on the PV in detail during the study of Costa, Diniz, and Kazmerski (2018). In Saudi Arabia, to remove the PV from deposited dust, they used jet water with low pressure, and the performance of the solar cell farm increased by 27% (Systems 2019). While the weak dust of density 0.644 g/m^2 reduced the performance of the PV by 7.4% (Chen et al. 2020). Various research on dust accumulation show results on how the different types of deposited dust particles will cause the decrease of the efficiency of the solar cells (Aljuhani et al. 2021; Alnasser et al. 2020; Chanchangi et al. 2020a, 2020b; Dhaouadi et al. 2021; Dida et al. 2020; Drame et al. 2021; Fan et al. 2021; Ilse et al. 2023; Javed et al. 2021; Kazem et al. 2020; Laarabi et al. 2021; Liu et al. 2021; Mustafa et al. 2020; Ullah et al. 2020; Zhang 2020). The rising temperature due to the high amount of solar radiation intensity caused a decrease in the PV cell's efficiency (Kazem and Chaichan 2019). The layering of the dust particles is mostly related to the temperature of the PV (Jaszczur 2019).

The PV of higher surface temperatures has lower accumulated dust (Gupta et al. 2019). The dust deposition on the PV's surface caused an increase in its surface temperature based on the study of Chaichan and Kazem (2020).

Cleaning the different panels is shown by the temperature-correction performance ratio (Guo et al. 2019). On the other hand, the cleaning process enhances the efficiency by 32.7% in a 1MWp PV farm (Hammoud et al. 2019). Based on the studies, the PV dust accumulation caused the thermal property settlement neither the electrical nor the optical (Gupta et al. 2019).

Finally, concentrating on complexity of dust distribution density and reduction power of PV panels, the researchers designed an experimental set up and measured the (I-V) and (P-V) data to evaluate the degree of dust accumulation on PV that exists in the environment. Firstly, the different types of dust samples are collected and each one is distributed on PV surface, the regular power production of PV panels is analysed, the basic equations form of dust density and power reduction rate is given, and dust density with irradiance is appointed. Basically, the analysis of the obtained behaviour of each of the five sample pollutants, containing distribution, concentration, composition, and the effect of dust particles on light transmission under different mass density and tilt angle is carried out. To ensure the reliability of the experimental results, some principle equations are used to to show the wrong analysis method for dust concentration.

The five-dust samples and their chemical decomposition are Toner (C) (Parthasarathy 2021), Cement (CaO, SiO_4) (Oliveira and Moreira 1989), Sand (AL_2O_3, SiO_4) (Ibbeken and Schleyer 1991), Soil, and Gypsum ($Ca_2SO_4.2H_2O_2$) (Bolukbasi, Kurt, and Palacio 2016). The basic contributions can be explored as follows:

- Different curve behaviour of dust particles and the reduction of power production at the same irradiance for obtaining the effect quantity of dust deposition are plotted.
- To guarantee the experimental process results, different scenarios are applied like irradiance reduction with respect to the dust distributed density, and influencing the coefficient of tilt angle for each of the five collected dust samples.
- The experimental and calculated results are in agreement.

TABLE I: NOMENCLATURE

Symbols	Meaning
PV	Photovoltaic
C	Carbon (Chemical decomposition of printer toner)
CaO, SiO_4	(Chemical decomposition of Cement)
AL_2O_3, SiO_4	(Chemical decomposition of Sand)
Ca_2SO_4	(Chemical decomposition of Gypsum)
R_{sh}	Shunt resistance of solar cell
Rs	Series resistance of solar cell
I_d	Diode current
Φ	Irradiance
$I_{\Phi 2}$	Light intensity current of clean PV
$I_{\Phi 3}$	Light intensity current of dusty PV
K	Boltzmann's constant
Si	Chemical abbreviation symbol of Silicon atom
Ge	Chemical abbreviation symbol of Germanium atom
T	Temperature
σ_{ext}	Extinction cross-sections coefficient
σ_{scat}	Scattering cross-sections coefficient
σ_{abs}	absorption cross-sections coefficient
b_{ext}	Extinction coefficient
b_{scat}	Scattering coefficient
b_{abs}	Absorption coefficient
ρ	Mass density (g/cm^2)
Φ_1	Irradiance intensity of sun
Φ_2	Irradiance intensity value after passing through plane glass
Φ_3	Irradiance intensity value after passing through plane glass and dusty glass
m	Mass of Sample dust
I	Current
A	Area (m^2)
η	Efficiency of PV
IR	Infrared radiation
$P_{max(dustyGlass)}$	Maximum power of dusty glass
$P_{max(clearGlass)}$	Maximum power of clear glass
x	Distance
W	Power Unit (Watt)
I	Current
V	Voltage

http://dx.doi.org/10.21622/RESD.2023.09.1.001

II. METHODOLOGY

A. *Position of the Problem*

As a basic reason that influences the output voltage (V) and output current (I) of PV, dust deposit on the solar panel can reduce the output power (I.V). The PV panel of internal circuit like Figure 1 is shown and the main parameters of V and I which affect the solar cell's actual power are described.

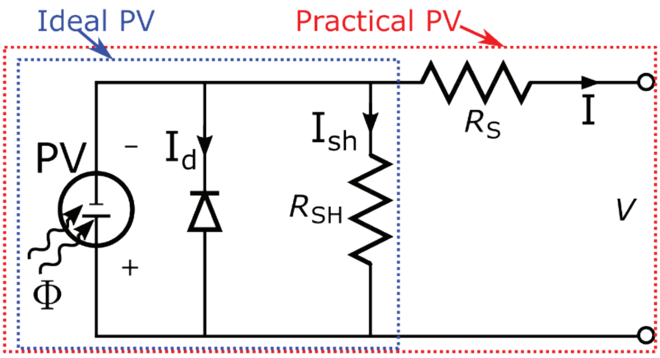

Fig.1. Solar Cell Internal Circuit

$$I_{\Phi_3} = I_{\phi 2} - I_0\left\{e^{\left[\frac{q(V+I_L R_S)}{n\times k\times T}\right]} - 1\right\} - \frac{V+I_L R_S}{R_{sh}} \quad (1)$$

Where I_{Φ_3}, $I_{\Phi 2}$ are light current, I_0 = saturate Current of diode, R_s is series resistor, K Boltzmann constant, T is temperature, n is constant (Kazem et al. 2022).

The influence of dust accumulation on reducing PV output power can affect the efficiency (η) and it can be described as:

$$\eta = \frac{P_{max}}{Pin} \times 100\% \quad (2)$$

Where P_{max} is output power of PV cell that is usually determined by measuring the output voltage V and output current I. P_{in} is input power of light to the PV which is (irradiance × Area of PV) (Ali et al. 2021).

B. *Study Area*

Continuously, the experimental process is done in the Halabja city-Kurdistan region of Iraq, as shown on 1st and 2nd October 2022. This city has an altitude angle and the azimuth angles are 35° and 5° (Jaafar and Maarof 2022).

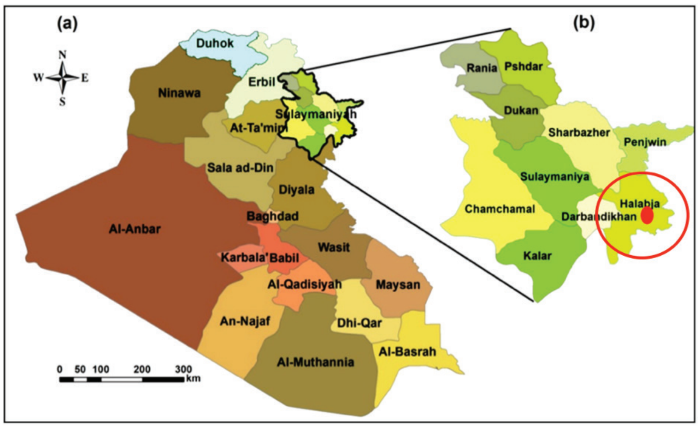

Fig.2. Location of Halabja City on Map (a) Iraq Map (B) Halabja and Sulaymaniyah Provinces (Halabja City (Zakaria et al. 2013)

Naturally, this location and in general most of the Iraqi provinces are under influence of dusty air in some months of year because of the existence of desert land in Iraq and other neighbouring countries. More than this, due to industrial actives, the same types of the collected dust pollutant exist in the environment air. For that reason, these kinds of the pollutants are collected and experimentally analysed to determine their effect on decreasing the PV performance.

Now, to have more accurate analysis data on dust accumulation on surface of PV, the calculation of the output power is usually done for the case of dusty surface (P_{dusty}) and clean surface (P_{clean}). After that the researchers defined the power reduction rate, which is used to present the best achieved efficiency (Ullah et al. 2020). Thus

$$L(t) = \frac{P_{clean} - P_{dusty}}{P_{clean}} \times 100\% \quad (3)$$

Where b_{ext} is the extinction factor due to the dust particles, the P_{dusty} is the output power of dusty panel and P_{clean} is output power of clean PV panel.

For having more detail and raising the level of accuracy the b_{ext} can be calculated as dependent on and represent as:

$$\Phi_3 = \Phi_2 e^{-(b_{ext}.x.\rho)} \quad (4)$$

Remark: For increasing the level of accuracy and test the next pollutants the previous one was totally removed from the surface of the PV. When the extinction coefficient of used plane glass b_{ext} 0.028, it can be easy to measure the reduced irradiance for each dust samples with different mass density.

The extinction coefficient can be determined from both scattered and absorption coefficient as (Redmond, Dial, and Thompson 2010):

$$b_{ext} = b_{scat} + b_{abs} \quad (5)$$

Where b_{scat}, b_{abs} is scattered and absorption coefficient, respectively.

Due to absorption) coefficient of dust particle the intensity of light reduced, then Lambert's Law stated as:

$$\Phi_3 = \Phi_2 e^{-(\mu x)} \quad (6)$$

Where is the intensity reduced due to (dusty PV), initial intensity of light after pass through clean PV and x is the interaction distance between the light and the dust particles.

C. *Experimental Setup*

After establishing the basic theory of experimental process, five prepared dust particles on PV panels in different amount of masses are investigated. Mainly, to detect the exact effectiveness coefficient b_{ext} and the reduced actual power, a real design of experiment is designed.

http://dx.doi.org/10.21622/RESD.2023.09.1.001

D. Experimental Process

Dust accumulation on PV cell in the real environment, a single PV panel of 15W power generation for experiment setup is set up. The dust samples and experiment set up are given in Figures 3 and 4.

In the first part, a plane glass is used to put on the PV surface. The aim of that was just for measuring the irradiance after going through the plane glass and the accumulated dust on plane glass. After that an outdoor PV power generation system is established. Three radiation levels are measured during the experiment, and the sun radiation range was from 925 to 1000 W/m^2 and this rang was between 560 to 700 W/m^2 for plane glass. In the second part, an electronic balance is used to calculate the dust mass density of the plane glass sheet. Here, it was necessary to control the mass of deposited pollutants in the third part, so that dust density range is 0.2840 g/cm^2 to 1.4198 g/cm^2. In the third part, the dust distributing process is done manually. Regarding to the non-uniform distribution of dust, it will have the same effect on the PV power same as the natural uniform deposition. After determining dust density and output power from the plotted curves, the effect model of dust accumulation and power efficiency is analyzed and obtained and the validity of the experiment is proved by the actual conditions.

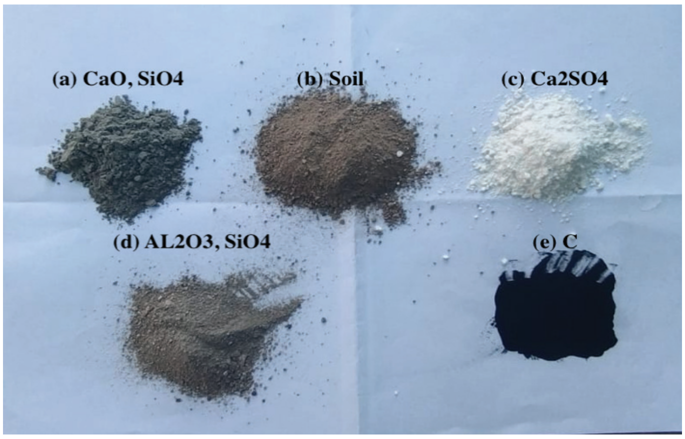

Fig.3. Different Samples of Dust Particles (a) CaO, SiO4 (b) Soil (c) Ca_2SO_4 (d) AL_2O_3, SiO_4 (e) C

Each type of dust pollutants is subjected to two of its chemical decomposition. Different dust masses are used for each sample, resulting in five levels of each sample. The density of each deposited dust is in a specific range. When the density is low, it has less influence on the power of PV panels. To keep going forward with the output power reduction, more dust pollutants are tested. The researchers appropriately increased the density of deposited dust sample. The accumulation steps are as follows:

Step 1. Measure the light irradiance directly from the sun, then measure it again after going through plane glass and finally for the third time after depositing the dust on the glass surface the irradiance is measured behind dusty plane glass.

Step 2. Lie the PV panel face up and put the plane glass on it and an area is specified by a marker in order not to deposit the dust out of PV panel area in case of high accuracy of dust influence on panel efficiency.

Step 3. By using voltmeter, ammeter, and a rheostat all V-I data are measured and the power is obtained for each couple I and V data. P-V curves are plotted as can be seen in Fig. 6.

Step 4. For all type of dusts with specific mass density different tilt angle 0° to 45° and for C case extra angle of 60° are tested. Step 3 is repeated for all tilt angle and the data are plotted.

To reduce the error factor of the experiments process, the steps are repeated on two continuous days in same natural conditions.

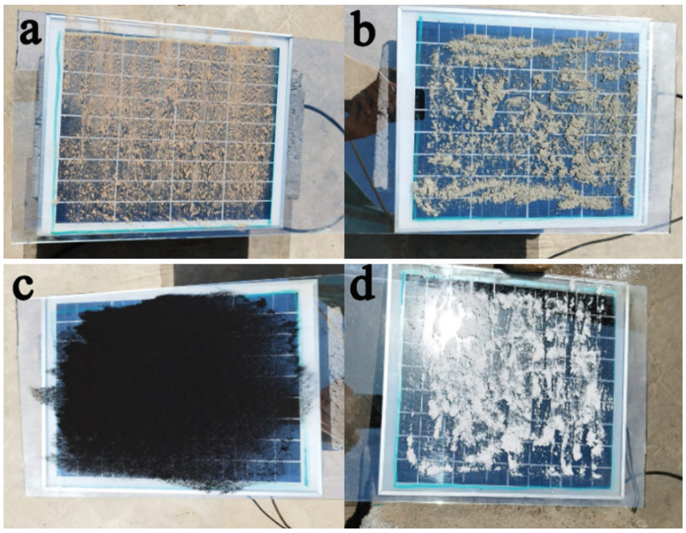

Fig.4. a: Soil and b: CaO,SiO2 c: C, d: $Ca_2SO_42H_2O_2$ Deposited of PV Surface

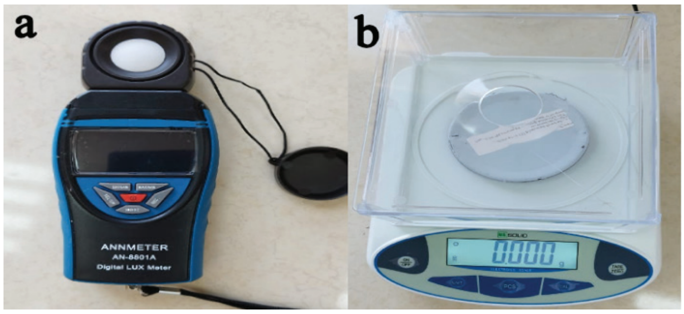

Fig.5. a: Digital Lux Meter, b: Electronics Balance Device

III. RESULTS AND DISCUSSION

In this part, the experimental outcome will be analyzed in detail. In subsection 5.1, the all parameters characteristics such as V-I curve, V-P curve, , , and different tilt angle of five dust pollutants are investigated.

A. *Analysis Impact of Dust Deposition on PV Panels*

In order to acquire the power reduction factor, the experiment is set up to test and measure the energy performance of the PV panel, including output voltage, current, power, irradiance and tilt angle. Fig. 6 shows the power output curves for all dust pollutants under unchanged radiation with a dust density of five levels. In addition, each sub-Figure shows the evolution of the power efficiency of the same dust pollutant of different

Volume 9, Issue 1, June 2023 - ISSN 2356-8569
http://dx.doi.org/10.21622/RESD.2023.09.1.001

mass (five concentrations of pollutant accumulation). Experimental results show that the output power of the PV panels decreases in different degrees with the increase of mass density of each accumulation effect.

At low density, the coverage area of toner on PV is more, which has high effect on power output. When the concentration of toner reaches 0.775 g/cm^2, the output power drops to zero. When the soil concentration raised to the same value, the output power changes to 2.4 W and it is significantly lower than the power of clean PV. The output power is 2.86 W, when the maximum density is 1.4119 g/cm^2 for Al_2O_3, SiO_4. CaO, SiO_4 is one of the pollutants that have reduce the output power to 2.17 W of the same density as Al_2O_3, SiO_4. It can be sensed that the output power of PV panels is highly sensitive to toner pollutant because of the its colour and adhesion.

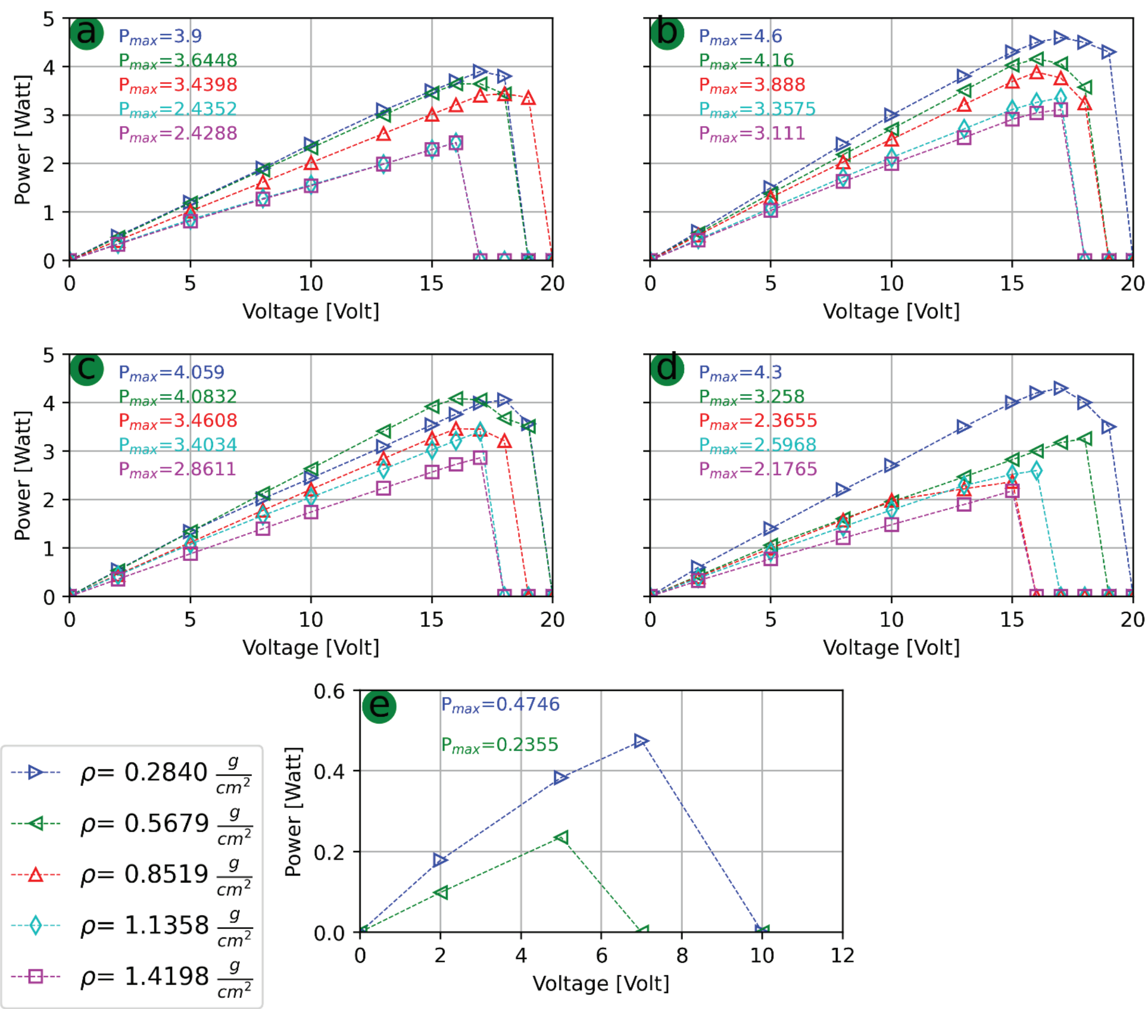

Fig.6. V-P Curves Characterization a: Soil, b: $Ca_2SO_4.2H_2O$, c:,AL_2O_3, SiO_2 d: CaO,SiO_2,

e: C.

From Fig. 7, the **plot (a):** represents five different curves of the same mass density. When the density is 0.5679 g/cm^2, the power decline trend is 62.35%, 66.95%, 69.05%, 63.35% and 96.65% for soil, (Al_2O_3, SiO_4), (CaO, SiO_4), ($Ca_2SO_4.2H_2O$) and (C), respectively. **Plot (b):** among all pollutants, soil, ($Ca_2SO_4.2H_2O$) and (Al_2O_3, SiO_4) rapidly changed with increasing the concentration. However, for (CaO, SiO_4), the output power extremely decreased from 0.28 g/cm^2 to 0.56 g/cm^2 and after that the change went slowly. For toner, output power rapidly goes to zero by concentration of 0.56 g/cm^2. **Plot (c):** soil, (Al_2O_3, SiO_4) and (CaO, SiO_4) by increasing the tilt angle, the effectiveness of their concentration will be reduced because the output power of each of the three increased. The output power increased highly after angle of 30° due to low adhesion. Toner C has a small particle size and high adhesion, and the output power goes forward constantly. **Plot (d):** toner pollutant highly reduced the irradiance, but other types of dust uniformly decreased the irradiance. The low concentration of pollutants has a little effect on irradiance, while high concentration of each influenced the irradiance significantly.

http://dx.doi.org/10.21622/RESD.2023.09.1.001

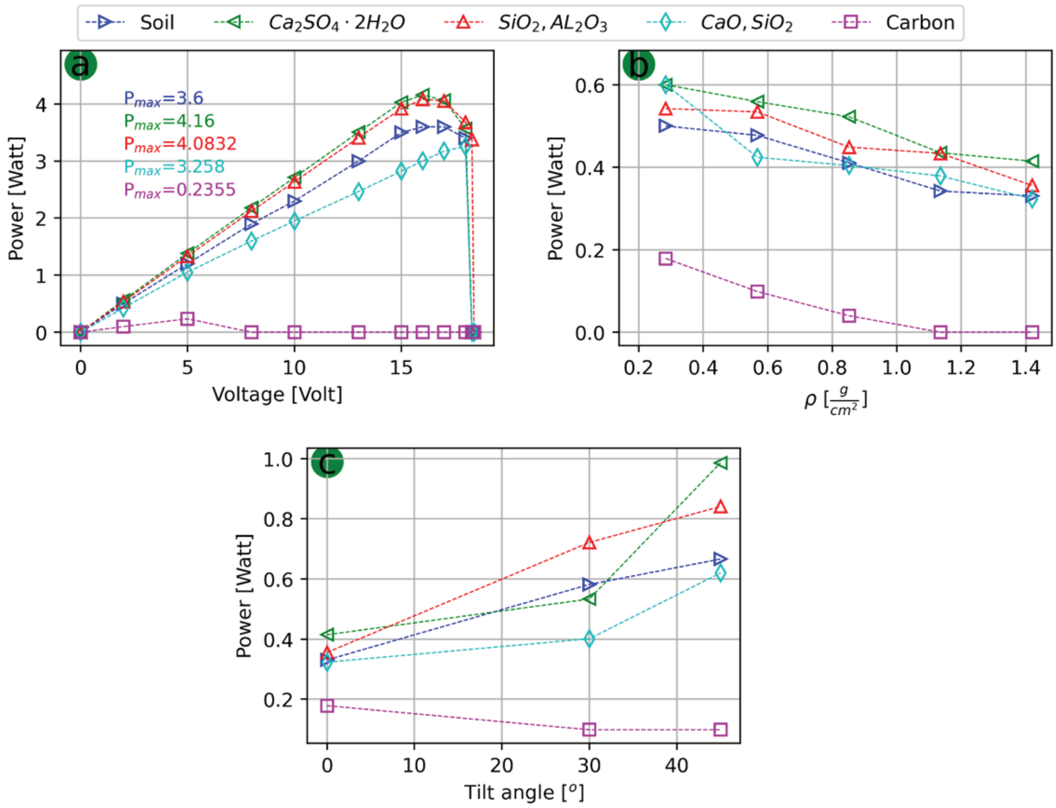

Fig.7. Curves of All Pollutants a: P - V curves, b: P – ρ curves c: P – tilt angle curve

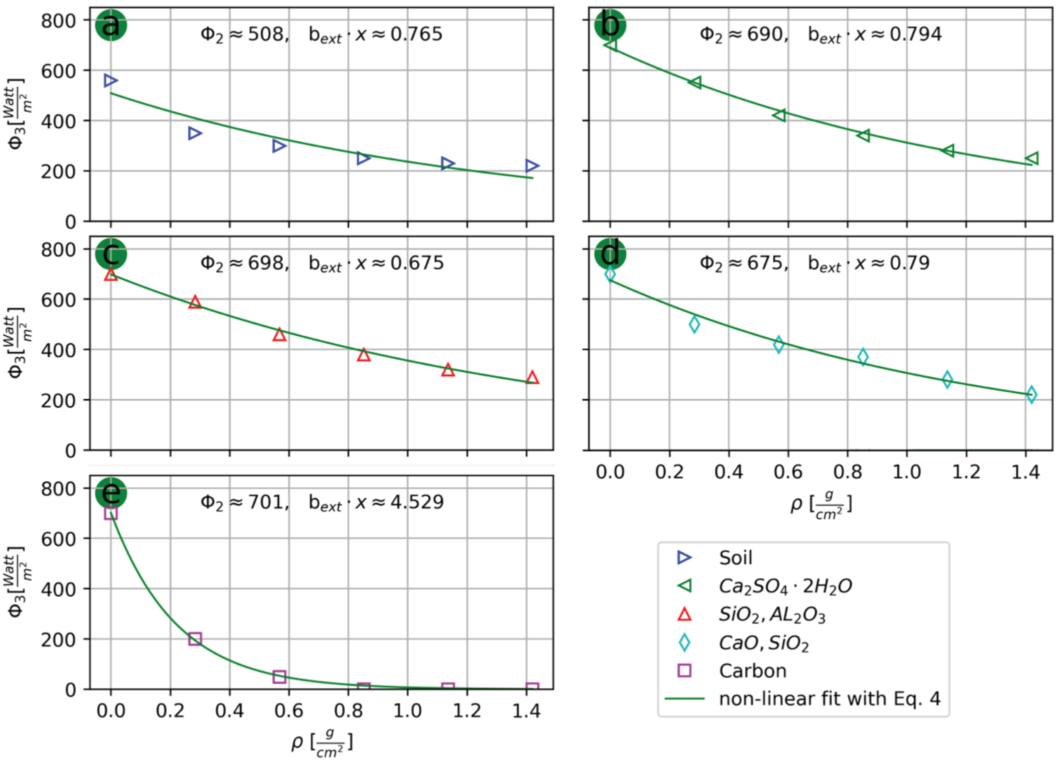

Fig.8. Φ_3 –ρ Curves with their Fitting Curves to Find the Value of bext .x

IV. CONCLUSIONS

The impact of five collected dust pollutants (Toner (C), Soil, Cement (CaO, SiO_4), Gypsum ($Ca_2SO_4.2H_2O$), and Sand (AL_2O_3, SiO_4) on the actual power of PV panels are determined in this study. Fortunately, the effectiveness of extinction coefficient of various dust particles for different dust decomposition on the power of PV panels with various concertation is determined. The overall the results could be as:

1. Dust deposition has a remarkable inhibitory influence on PV panels output power, and its efficiency debilitation depends on the kind of pollutant colour, composition, and more on the density of dusts.
2. Joining the impact of concentration on the irradiance ratio of PV panels output power experimentally established.
3. The outcomes present that the calculated output power reduced (62% to 96%), irradiance (34% to 93%) decreased and increasing of output power due to increasing of tilt angle as redouble the power, But toner double down the power.
4. The extinction coefficient of all pollutants has been found and the toner has the highest extinction with (AL_2O_3, SiO_4).

Although the influence of different dusts is collected, their accumulation on the PV is considerably not uniformly, and there may be difference extinction coefficient various points on PV panel. In the future, the used model of uniform distribution condition of pollutant should be further developed to have a uniform experimental process for the recording of V-I and V-P graphs of pollutants.

Contribution

Saman Jaafar carried out system building, data analysis, and interpretation experiments. Hiwa Abdlla Maarof and Renas T Salh cooperated as a partner in data analysis. Hoshang Sahib did the plots and fitting of the data measures. Yousif Azeez cooperated as paraphrasing and rewrite the draft version. All authors have read and agreed to the published version of the manuscript.

Declarations

Ethical approval and consent to participate: Not applicable.

Consent for publication: Not applicable.

Conflicts of interest: The authors declare no conflict of interest

References

[1] M. Al-Housani, Y. Bicer, and M. Koç, "Assessment of various dry photovoltaic cleaning techniques and frequencies on the power output of CdTe-type modules in dusty environments," Sustainability (Switzerland), vol. 11, no. 10, 2019, doi: 10.3390/su11102850.

[2] S. Ali Sadat, J. Faraji, M. Nazififard, and A. Ketabi, "The experimental analysis of dust deposition effect on solar photovoltaic panels in Iran's desert environment," Sustainable Energy Technologies and Assessments, vol. 47, 2021, doi: 10.1016/j.seta.2021.101542.

[3] M. Aljuhani, M. R. Gomaa, T. S. Mandourah, and M. A. Mowffaq, "The Environmental Effects on the Photovoltaic Panel Power : Jeddah Case Study," vol. 44, no. 6, pp. 251–262, 2021.

[4] T. M. A. Alnasser, A. M. J. Mahdy, K. I. Abass, M. T. Chaichan, and H. A. Kazem, "Impact of dust ingredient on photovoltaic performance: An experimental study," Solar Energy, vol. 195, 2020, doi: 10.1016/j.solener.2019.12.008.

[5] Y. Andrea, T. Pogrebnaya, and B. Kichonge, "Effect of Industrial Dust Deposition on Photovoltaic Module Performance: Experimental Measurements in the Tropical Region," International Journal of Photoenergy, vol. 2019, 2019, doi: 10.1155/2019/1892148.

[6] M. Benghanem, A. Almohammedi, M. Taukeer Khan, and A. A. Al-Mashraqi, "Effect of dust accumulation on the performance of photovoltaic panels in desert countries: A case study for Madinah, Saudi Arabia," International Journal of Power Electronics and Drive Systems, vol. 9, no. 3, 2018, doi: 10.11591/ijpeds.v9.i3.pp1356-1366.

[7] A. Bolukbasi, L. Kurt, and S. Palacio, "Unravelling the mechanisms for plant survival on gypsum soils: An analysis of the chemical composition of gypsum plants from Turkey," Plant Biol, vol. 18, no. 2, 2016, doi: 10.1111/plb.12401.

[8] M. T. Chaichan and H. A. Kazem, "Environmental Effects Experimental evaluation of dust composition impact on photovoltaic performance in Iraq," Energy Sources, Part A Recover. Util. Environ. Eff., vol. 00, no. 00, pp. 1–22, 2020, doi: 10.1080/15567036.2020.1746444.

[9] Y. N. Chanchangi, A. Ghosh, S. Sundaram, and T. K. Mallick, "An analytical indoor experimental study on the effect of soiling on PV, focusing on dust properties and PV surface material," Solar Energy, vol. 203, 2020, doi: 10.1016/j.solener.2020.03.089.

[10] Y. N. Chanchangi, A. Ghosh, S. Sundaram, and T. K. Mallick, "Dust and PV Performance in Nigeria: A review," Renewable and Sustainable Energy Reviews, vol. 121. 2020. doi: 10.1016/j.

rser.2020.109704.

[11] J. Chen, G. Pan, J. Ouyang, J. Ma, L. Fu, and L. Zhang, "Study on impacts of dust accumulation and rainfall on PV power reduction in East China," Energy, vol. 194, 2020, doi: 10.1016/j.energy.2020.116915.

[12] Y. Chen et al., "Experimental study on the effect of dust deposition on photovoltaic panels," in Energy Procedia, 2019, vol. 158. doi: 10.1016/j.egypro.2019.01.139.

[13] S. C. S. Costa, A. S. A. C. Diniz, and L. L. Kazmerski, "Solar energy dust and soiling R&D progress: Literature review update for 2016," Renewable and Sustainable Energy Reviews, vol. 82. 2018. doi: 10.1016/j.rser.2017.09.015.

[14] R. Dhaouadi, A. Al-Othman, A. A. Aidan, M. Tawalbeh, and R. Zannerni, "A characterization study for the properties of dust particles collected on photovoltaic (PV) panels in Sharjah, United Arab Emirates," Renew Energy, vol. 171, 2021, doi: 10.1016/j.renene.2021.02.083.

[15] M. Dida, S. Boughali, D. Bechki, and H. Bouguettaia, "Output power loss of crystalline silicon photovoltaic modules due to dust accumulation in Saharan environment," Renewable and Sustainable Energy Reviews, vol. 124, 2020, doi: 10.1016/j.rser.2020.109787.

[16] M. S. Drame, D. Diop, K. Talla, M. Diallo, B. D. Ngom, and B. Nebon, "Structural and physicochemical properties of dust collected on PV panels surfaces and their potential influence on these solar modules efficiency in Dakar, Senegal, West Africa," Sci Afr, vol. 12, 2021, doi: 10.1016/j.sciaf.2021.e00810.

[17] S. Fan, Y. Wang, S. Cao, T. Sun, and P. Liu, "A novel method for analyzing the effect of dust accumulation on energy efficiency loss in photovoltaic (PV) system," Energy, vol. 234, 2021, doi: 10.1016/j.energy.2021.121112.

[18] B. Guo, W. Javed, Y. S. Khoo, and B. Figgis, "Solar PV soiling mitigation by electrodynamic dust shield in field conditions," Solar Energy, vol. 188, 2019, doi: 10.1016/j.solener.2019.05.071.

[19] V. Gupta, M. Sharma, R. K. Pachauri, and K. N. Dinesh Babu, "Comprehensive review on effect of dust on solar photovoltaic system and mitigation techniques," Solar Energy, vol. 191. 2019. doi: 10.1016/j.solener.2019.08.079.

[20] A. A. Hachicha, I. Al-Sawafta, and Z. Said, "Impact of dust on the performance of solar photovoltaic (PV) systems under United Arab Emirates weather conditions," Renew Energy, vol. 141, 2019, doi: 10.1016/j.renene.2019.04.004.

[21] M. Hammoud, B. Shokr, A. Assi, J. Hallal, and P. Khoury, "Effect of dust cleaning on the enhancement of the power generation of a coastal PV-power plant at Zahrani Lebanon," Solar Energy, vol. 184, 2019, doi: 10.1016/j.solener.2019.04.005

[22] H. Ibbeken and R. Schleyer, "Development of the Chemical Composition of Sand," Source and Sediment, pp. 112–123, 1991, doi: 10.1007/978-3-642-76165-2_10.

[23] K. Ilse et al., "Techno-Economic Assessment of Soiling Losses and Mitigation Strategies for Solar Power Generation," Joule, vol. 3, no. 10. 2019. doi: 10.1016/j.joule.2019.08.019.

[24] R. J. Isaifan, D. Johnson, L. Ackermann, B. Figgis, and M. Ayoub, "Solar Energy Materials and Solar Cells Evaluation of the adhesion forces between dust particles and photovoltaic module surfaces," Sol. Energy Mater. Sol. Cells, vol. 191, no. March 2018, pp. 413–421, 2019, doi: 10.1016/j.solmat.2018.11.031.

[25] S. S. Jaafar and H. A. Maarof, "Influence of Micro-Controller-Based Single Axis Solar Tracker System on Solar Panel ' s Performance : Case Study Influence of Micro-Controller-Based Single Axis Solar Tracker System on Solar Panel ' s Performance : Case Study," no. September, 2022.

[26] M. Jaszczur et al., "The field experiments and model of the natural dust deposition effects on photovoltaic module efficiency," Environmental Science and Pollution Research, vol. 26, no. 9, 2019, doi: 10.1007/s11356-018-1970-x.

[27] M. Jaszczur, A. Koshti, W. Nawrot, and P. Sędor, "An investigation of the dust accumulation on photovoltaic panels," Environmental Science and Pollution Research, vol. 27, no. 2, 2020, doi: 10.1007/s11356-019-06742-2.

[28] W. Javed, B. Guo, B. Figgis, and B. Aïssa, "Dust potency in the context of solar photovoltaic (PV) soiling loss," Solar Energy, vol. 220, 2021, doi: 10.1016/j.solener.2021.04.015.

[29] H. Kawamoto and B. Guo, "Improvement of an electrostatic cleaning system for removal of dust from solar panels," J Electrostat, vol. 91, 2018, doi: 10.1016/j.elstat.2017.12.002.

[30] H. A. Kazem, A. H. A. Al-Waeli, M. T. Chaichan, and K. Sopian, "Modeling and experimental validation of dust impact on solar cell performance," Energy Sources, Part A: Recovery,

Utilization and Environmental Effects, 2022, doi: 10.1080/15567036.2021.2024922.

[31] H. A. Kazem and M. T. Chaichan, "The effect of dust accumulation and cleaning methods on PV panels' outcomes based on an experimental study of six locations in Northern Oman," Solar Energy, vol. 187, 2019, doi: 10.1016/j.solener.2019.05.036.

[32] H. A. Kazem, M. T. Chaichan, A. H. A. Al-Waeli, and K. Sopian, "A review of dust accumulation and cleaning methods for solar photovoltaic systems," Journal of Cleaner Production, vol. 276. 2020. doi: 10.1016/j.jclepro.2020.123187.

[33] A. Khodakaram-Tafti and M. Yaghoubi, "Experimental study on the effect of dust deposition on photovoltaic performance at various tilts in semi-arid environment," Sustainable Energy Technologies and Assessments, vol. 42, 2020, doi: 10.1016/j.seta.2020.100822.

[34] B. Laarabi, Y. el Baqqal, N. Rajasekar, and A. Barhdadi, "Updated review on soiling of solar photovoltaic systems Morocco and India contributions," Journal of Cleaner Production, vol. 311. 2021. doi: 10.1016/j.jclepro.2021.127608.

[35] X. Liu, S. Yue, L. Lu, and J. Li, "Investigation of the Dust Scaling Behaviour on Solar Photovoltaic Panels," J Clean Prod, vol. 295, 2021, doi: 10.1016/j.jclepro.2021.126391.

[36] R. D. Lorenz et al., "Scienti fi c Observations With the InSight Solar Arrays : Dust , Clouds , and Eclipses on Mars," vol. 200, no. June, pp. 1–12, 2019, doi: 10.1029/2019EA000992.

[37] F. M. Mahmood, S. S. Jaafar, and R. W. Mustafa, "Designing and programming a microcontroller based on a solar tracking system," vol. 3, no. 1, pp. 51–59, 2022.

[38] M. Memiche, C. Bouzian, A. Benzahia, and A. Moussi, "Effects of dust, soiling, aging, and weather conditions on photovoltaic system performances in a Saharan environment—Case study in Algeria," Global Energy Interconnection, vol. 3, no. 1, 2020, doi: 10.1016/j.gloei.2020.03.004.

[39] M. Mostefaoui, A. Ziane, A. Bouraiou, and S. Khelifi, "Effect of sand dust accumulation on photovoltaic performance in the Saharan environment: southern Algeria (Adrar)," Environmental Science and Pollution Research, vol. 26, no. 1, 2019, doi: 10.1007/s11356-018-3496-7.

[40] M. Mussard and M. Amara, "Performance of solar photovoltaic modules under arid climatic conditions: A review," Solar Energy, vol. 174. 2018. doi: 10.1016/j.solener.2018.08.071.

[41] R. J. Mustafa, M. R. Gomaa, M. Al-Dhaifallah, and H. Rezk, "Environmental impacts on the performance of solar photovoltaic systems," Sustainability (Switzerland), vol. 12, no. 2, 2020, doi: 10.3390/su12020608.

[42] F. L. G. Oliveira and M. I. R. Moreira, "CHEMICAL COMPOSITION OF CEMENT PORE SOLUTIONS," J. Japan Soc. Air Pollut., vol. 24, no. 1, pp. 45–51, 1989.

[43] M. F. Shaaban, A. Alarif, M. Mokhtar, U. Tariq, A. H. Osman, and A. R. Al-Ali, "A new data-based dust estimation unit for pv panels," Energies (Basel), vol. 13, no. 14, 2020, doi: 10.3390/en13143601.

[44] B. Parrott, P. Carrasco Zanini, A. Shehri, K. Kotsovos, and I. Gereige, "Automated, robotic dry-cleaning of solar panels in Thuwal, Saudi Arabia using a silicone rubber brush," Solar Energy, vol. 171, 2018, doi: 10.1016/j.solener.2018.06.104.

[45] M. Parthasarathy, "Challenges and emerging trends in toner waste recycling: A review," Recycling, vol. 6, no. 3. 2021. doi: 10.3390/recycling6030057.

[46] H. E. Redmond, K. D. Dial, and J. E. Thompson, "Light scattering and absorption by wind blown dust: Theory, measurement, and recent data," Aeolian Research, vol. 2, no. 1. 2010. doi: 10.1016/j.aeolia.2009.09.002.

[47] S. A. M. Said, G. Hassan, H. M. Walwil, and N. Al-Aqeeli, "The effect of environmental factors and dust accumulation on photovoltaic modules and dust-accumulation mitigation strategies," Renewable and Sustainable Energy Reviews, vol. 82. 2018. doi: 10.1016/j.rser.2017.09.042.

[48] H. Salimi, H. Ahmadi, D. Ashtiani, A. Mirabdolah, and R. Fazaeli, "Environmental Effects Experimental analysis and modeling of weather condition effects on photovoltaic systems ' performance : Tehran case study," Energy Sources, Part A Recover. Util. Environ. Eff., vol. 00, no. 00, pp. 1–13, 2020, doi: 10.1080/15567036.2020.1765902.

[49] A. Ullah, A. Amin, T. Haider, M. Saleem, and N. Z. Butt, "Investigation of soiling effects, dust chemistry and optimum cleaning schedule for PV modules in Lahore, Pakistan," Renew Energy, vol. 150, 2020, doi: 10.1016/j.renene.2019.12.090.

[50] P. Wang et al., "Reducing the effect of dust deposition on the generating efficiency of solar PV modules by super-hydrophobic films," Solar Energy, vol. 169, 2018, doi: 10.1016/j.solener.2017.12.052.

[51] L. Xingcai and N. Kun, "Effectively predict the solar radiation transmittance of dusty photovoltaic panels through Lambert-Beer law," Renew Energy, vol. 123, 2018, doi: 10.1016/j.renene.2018.02.046.

[52] S. Zakaria, Y. T. Mustafa, D. A. Mohammed, S. S. Ali, N. Al-Ansari, and S. Knutsson, "Estimation of annual harvested runoff at Sulaymaniyah Governorate, Kurdistan region of Iraq," Nat Sci (Irvine), vol. 05, no. 12, 2013, doi: 10.4236/ns.2013.512155.

[53] L. zhi Zhang, A. jian Pan, R. rong Cai, and H. Lu, "Indoor experiments of dust deposition reduction on solar cell covering glass by transparent super-hydrophobic coating with different tilt angles," Solar Energy, vol. 188, 2019, doi: 10.1016/j.solener.2019.07.026.

[54] X. Li, T. Liu, J. Wang, L. Xu, and Z. Zhang, "Dust deposition can focus light at a limited distance on photovoltaic panels," J Quant Spectrosc Radiat Transf, vol. 246, 2020, doi: 10.1016/j.jqsrt.2020.106921.

Journal of Renewable Energy and Sustainable Development (RESD) Volume 9, Issue 1, June 2023 - ISSN 2356-8569
http://dx.doi.org/10.21622/RESD.2023.09.1.011

Received on, 11 January 2023 Accepted on, 03 May 2023 Published on, 30 May 2023

Power Density Improvement Due To Rotor Flux Screens In An Srm With A Higher Number Of Rotor Poles Than Stator Poles

Ali A. Abdel-Aziz[1], Khaled H. Ahmed[1, 2], Ahmed M. Massoud[3] and Barry W. Williams[1]

[1]Departement of Electronic and Electrical Engineering, University of Strathclyde, Glasgow, G1 1XQ, UK
[2]Department of Electrical Engineering, Alexandria University, Alexandria, 21544, Egypt
[3] Department of Electrical Engineering, Qatar University, Doha, P.O. Box 2713, Qatar

Emails: ali.hassan-abdelaziz-ali@strath.ac.uk, khaled.ahmed@strath.ac.uk, ahmed.massoud@qu.edu.q, barry.williams@strath.ac.uk

ABSTRACT

This paper studies the performance of screened switched reluctance motors (SRMs) with a number of rotor poles higher than the number of stator poles. Flux (conducting) screens are electrically conducting, non-magnetic materials like aluminum or copper. These screens fill the interpolar rotor air gaps decreasing the unaligned inductance, and thereby increasing the output torque. In addition, flux screens result in a cylindrical rotor structure which minimizes windage losses especially at high speeds. The paper investigates the effect of the flux screens thickness and material on the SRM performance including output torque, power and phase current. A modified flux tube approach for estimating the unaligned inductance of screened SRM is proposed. Finite element analysis results for different screen cases confirm the effectiveness of conducting screens in improving the torque, hence power capability, of switched reluctance motors.

Index-words: *Electric vehicles, Finite element analysis, Flux screens, Power density, Renewable energy, Switched reluctance motor, Torque ripple.*

I. INTRODUCTION

In recent years, there has been an increasing interest in replacing conventional fossil fuels for electrical energy generation with renewable energy resources to reduce pollution in an attempt to achieve a green environment. With the transportation sector being a major source of carbon dioxide emissions, researchers are oriented towards electrifying the transportation section [1].

Different electrical machines, including DC, synchronous, and induction machines could be used for propulsion [2], [3]. Conventionally, the first-choice traction machine is the permanent magnet synchronous machine (PMSM) due to its high torque density, and wide constant torque/speed range. However, escalated prices and restricted resources of rare-earth materials forced the market to look for a suitable, magnet-free alternative [4].

The switched reluctance machine (SRM) is the dark horse in this race [5]. It has a simple, robust structure, with low cost. Being a double-salient machine with concentrated winding on stator poles, and with neither windings nor permanent magnets on the rotor poles made its design and geometry simpler. Despite the SRM advantages, it suffers from two main drawbacks, namely, vibration and low power density when compared with other traction machines like the PMSM [6] - [8]. Recently, there have been decent attempts to improve the SRM power density [9], [10]. Improving the efficiency and the power density of the SRM to compete with the PMSM was achieved [11] - [13].

The SRM has been studied extensively in recent decades [14]. A new SRM trend explores a higher number of rotor poles than stator poles, as presented in [15]. The new motor concept (N_s<N_r) (N_s, N_r are the number of stator and rotor poles, respectively) has lower mass and copper loss than the conventional SRM (N_s>N_r). Due to the extra space available in the stator slot area, windings with a higher number of turns and thicker cross-sectional area can be deployed [16]. Also, the rotor pole number increase minimizes torque ripple, which is vital for electric vehicle (EV) applications [17]. However, since the interpolar rotor airgaps are narrower in the new motor design, there is an increase in the unaligned inductance value when compared to that of the conventional SRM. The increase of unaligned inductance reduces the energy conversion area, and hence the produced torque.

In addition, the process of current build-up in the stator winding will be slower due to the decrease in the unaligned inductance value [18]. Hence, to restore the speed of current build-up, a DC link voltage with higher magnitude is required. Also, the salient rotor structure increases the windage loss, especially at high speeds.

Rotor ribs are proposed in [19], [20], to mitigate the SRM windage loss. Film magnetic material is inserted between rotor poles; hence, producing a cylindrical rotor shape. Although the windage loss is significantly reduced, the torque density is reduced, and the torque ripple increased, in addition to the mechanical constraints imposed in fabricating the thin magnetic material.

Volume 9, Issue 1, June 2023 - ISSN 2356-8569
http://dx.doi.org/10.21622/RESD.2023.09.1.011

Segmented rotor SRM (SRSRM) with cylindrical rotor design was investigated [21]. However, it suffers from complexity in manufacturing and mechanical weaknesses [22]. In addition, the SRSRM has a longer end winding, which deteriorates the electrical loading of the motor [23]. Also, this motor is not suitable for applications requiring motors with short lamination stack length [24].

The concept of flux screens was proposed in [25]. Interpolar rotor air gaps are filled with materials like copper or aluminium which are electrically conducting materials with non-magnetic properties. When the rotor rotates with any speed, voltage is induced in the conducting screens, resulting in the flow of eddy currents. A magnetic field is set up by the flow of eddy currents, which opposes the stator main magnetic field. The result is a decrease in the unaligned inductance value. In [25], the impact of utilizing rotor conducting screens on a three-phase 6/4 SRM was investigated. The deployment of rotor conducting screens for three different SRMs was investigated in [26] – [28], where the screened machines produced higher torque levels than unscreened machines with equivalent volume. However, there was no attempt to investigate the SRM performance when varying the thickness or the material of the conducting screen. Also, the low number of rotor poles increases the torque ripple, which is undesirable for EV applications.

In this paper, the utilization of rotor conducting screens for an SRM with a higher number of rotor poles than stator poles ($N_r>N_s$) is investigated. The increased rotor pole number reduces torque ripple. The deployment of rotor conducting screens reduces the unaligned inductance value, hence allowing faster current build-up resulting in higher power per unit volume. Also, as with any SRM, filling the spaces between rotor poles mitigates the windage loss, especially at higher rotor speed. A detailed procedure using the flux tube method for calculating the effective value of unaligned inductance for screened SRMs is presented. Finally, the performance of screened SRM with different screen thicknesses and materials is assessed.

The paper is organized as follows. Section II sheds light on the concept of utilizing rotor conducting screens for SRMs. A method, based on flux tube approach, is discussed in section III to calculate the unaligned inductance value for screened SRM. Supporting 2D and 3D finite element analysis (FEA) results are presented in section IV.

II. SRM WITH ROTOR CONDUCTING SCREENS

The SRM structure is simple having salient stator and rotor poles. Only the stator poles have concentrated winding, where each two opposite poles are connected in series forming a phase. In the unaligned position, the flux linkage-current (λ-i) characteristics is linear as the core reluctance is much smaller than the air gap reluctance. On the other hand, when the SRM is in the aligned position core reluctance cannot be ignored resulting non-linear (λ-i) characteristics, as shown in Figure 1.

The conversion area OAB, which is the increase in co-energy when the rotor moves from the unaligned to the aligned position, controls the developed torque. Reducing the effective unaligned inductance increases the conversion area, hence increasing motor output torque. Equation (1) defines the torque.

$$T = \frac{\partial W_f'(\theta, i)}{\partial \theta} \tag{1}$$

where θ is the rotor position and W_f' is the co-energy

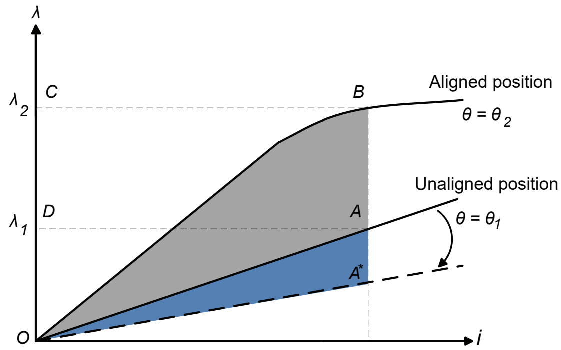

Fig. 1. Flux linkage-current (λ-i) characteristics of SRM

A new family of SRMs with a higher number of rotor poles than stator poles was presented as in literature. A three-phase 6/10 SRM and a four-phase 8/14 SRM are examples of the new concept. The new SRM can be operated using the traditional asymmetric half-bridge converter [29] and is characterized by reduced torque ripple since $Nr>Ns$, which results in an increased number of strokes per revolution whence increased phase overlap.

Figure 2 shows a three-phase 6/10 SRM. Where, D_{sh}, d, D are the shaft diameter, rotor diameter, and outer stator diameter, respectively. h_s, h_r are the stator and rotor pole heights, respectively. b_{sy} , b_{ry} are the stator and rotor back iron, respectively. β_s , β_r are the stator and rotor pole arcs, respectively. L_g is the air gap length, L is the stack length, and N is the number of turns per phase.

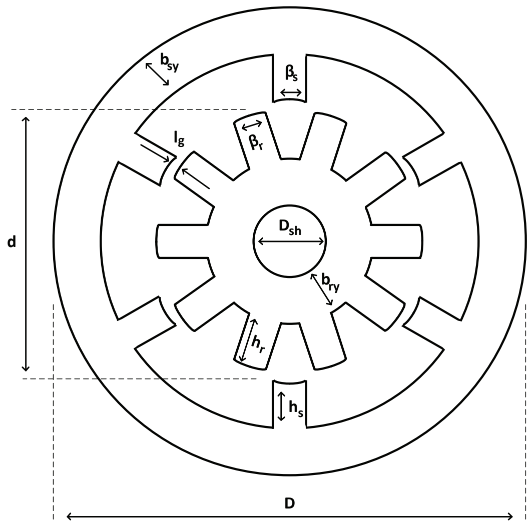

Fig. 2. Model of 6/10 SRM

 Volume 9, Issue 1, June 2023 - ISSN 2356-8569
http://dx.doi.org/10.21622/RESD.2023.09.1.011

For a high number of rotor poles, the available interpolar rotor spaces are narrower when compared with the traditional SRM. Thus, the unaligned inductance is high. Copper or aluminum, which are electrically conducting but non-magnetic materials, are utilized to fill in the interpolar rotor air gaps as shown in Figure 3. Whence, this material is referred to as a conducting screen. When the rotor rotates with any speed, voltage is induced in the conducting screens, resulting in the flow of eddy currents. A magnetic field is set up by the flow of eddy currents, which opposes the stator main magnetic field. The result is a decrease in the unaligned inductance.

III. FLUX TUBE APPROACH FOR UNALIGNED INDUCTANCE CALCULATION OF SCREENED-SRM

The unaligned inductance effective value is of paramount importance to predict the SRM performance [30]. FEA is an intuitive choice for designing and testing electrical machines. Nevertheless, in the early design stage any change in the SRM geometry, turns number or conduction period, will dictate a new model to be built and simulated. which is a time-consuming process. Hence, starting with a mathematical model is a wise choice which compromises both accuracy and time [31].

This section establishes the unaligned inductance calculation method of screened-SRM using the flux-tube approach [32]. It is worth mentioning that, at the aligned position the screens do not alter the aligned inductance. Five flux paths are used to describe the flux magnetic path at the unaligned position as illustrated in Figure 3.

Figure 4 demonstrates the magnetic equivalent circuit for calculating the screened-SRM unaligned inductance. Where, R_{sp},R_g,R_{rp}, R_{sy} and R_{ry} are the reluctances of the stator pole, air gap, rotor pole, stator back iron, and rotor back iron, respectively.

Flux path reluctances are calculated based on the machine geometrical dimensions. In the unaligned position, core reluctance is insignificant when compared to air gap reluctance. Hence, a linear flux linkage – current (λ - i) characteristics curve is obtained.

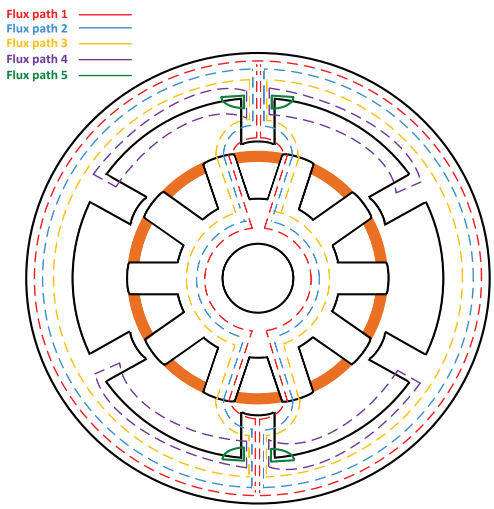

Fig. 3. Flux paths in unaligned position

Generally, reluctance could be expressed by [33], [34].

$$R = {}^{l}/_{\mu_0 \mu_r A} \tag{2}$$

where l is the flux magnetic-path length, A is the cross-sectional area, and μ_0 and μ_r are the permeability of air and core material relative permeability, respectively. The reluctances for the flux paths are derived in detail in the next subsections.

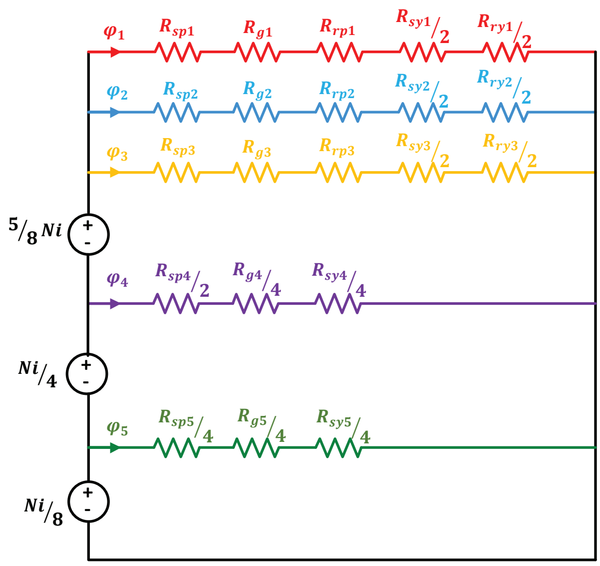

Fig 4. Magnetic equivalent circuit

A. *Flux Paths 1, 2 and 3*

The first three flux tubes are similar. Hence, their analysis is combined in this subsection. Figure 5 shows the first magnetic flux path where flux flows through the rotor back iron, the stator back iron, the rotor pole, the stator pole, and finally, the interpolar rotor air gap. Five reluctances are used to describe the magnetic flux path. The magnetic-flux path length and cross-sectional area are calculated as follows:

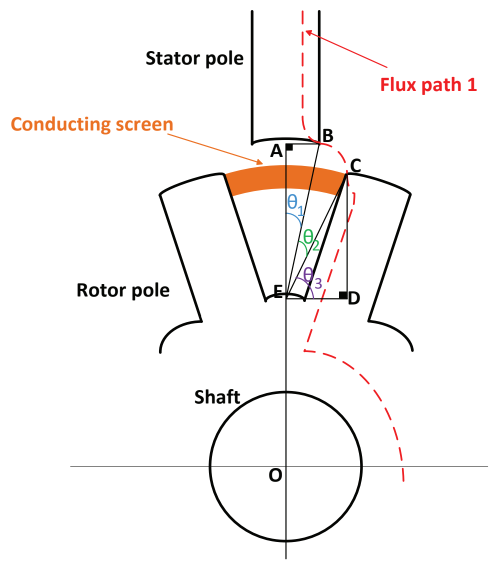

Fig. 5. Flux path 1

Volume 9, Issue 1, June 2023 - ISSN 2356-8569
http://dx.doi.org/10.21622/RESD.2023.09.1.011

1. Rotor Back Iron Reluctance, R_{ry1}, R_{ry2}, R_{ry3}

For rotor back iron, the average magnetic flux path length and the cross-sectional area are defined by (3) and (4), respectively.

$$l_{ryx} = ½\pi\{D_{sh} + b_{ry}\} \tag{3}$$

$$A_{ryx} = L\, b_{ry} \tag{4}$$

where, x =1, 2, 3 represents flux paths 1, 2 and 3, respectively.

2. Stator Back Iron Reluctance, R_{sy1}, R_{sy2}, R_{sy3}

Equations (5) and (6) define the average magnetic flux path length and the cross-sectional area for the stator back iron.

$$l_{syx} = ½\pi\{D - b_{sy}\} \tag{5}$$

$$A_{sx} = L\, b_{sy} \tag{6}$$

3. Rotor Pole Reluctance, R_{rp1}, R_{rp2}, R_{rp3}

For the first three flux paths, the flux travels through the entire rotor pole height. Hence, the average magnetic flux path length is given by (7), where (8) defines the cross-sectional area.

$$l_{rpx} = h_r \tag{7}$$

$$A_{rpx} = \begin{cases} L(½d - l_g)⅜\beta_r^{rad} & ,flux\ path\ 1 \\ L(½d - l_g)½\beta_r^{rad} & ,flux\ path\ 2 \\ L(½d - l_g)⅛\beta_r^{rad} & ,flux\ path\ 3 \end{cases} \tag{8}$$

4. Stator Pole Reluctance, R_{sp1}, R_{sp2}, R_{sp3}

For path 1, the flux is assumed to leave the stator at the pole tip. For paths 2 and 3, the flux is assumed to leave the stator at ⅒ and ¾ of the stator pole height from the top, respectively. Hence, the length of the flux path is defined by (9).

The width of the flux path determines the area. For flux path 1, the area is assumed to have width ½ β_s+¼ h_s. For paths 2 and 3, the entire flux flows throughout the pole height at a width ½ h_s and ⅛ h_s, respectively. The area is then defined by (10).

$$l_{spx} = \begin{cases} h_s & ,flux\ path\ 1 \\ 0.9h_s & ,flux\ path\ 2 \\ ¼h_s & ,flux\ path\ 3 \end{cases} \tag{9}$$

$$A_{spx} = \begin{cases} L(½d\beta_s^{rad} + ¼h_s) & ,flux\ path\ 1 \\ ½Lh_s & ,flux\ path\ 2 \\ ⅛Lh_s & ,flux\ path\ 3 \end{cases} \tag{10}$$

5. Air Gap Reluctance, R_{g1}, R_{g2}, R_{g3}

The average magnetic flux path length for the air gap is the arc BC as illustrated in Figure 5 and defined by (11)

$$l_{gx}=BC=½(EB+EC)\ \theta_2^{rad} \tag{11}$$

When calculating the cross-sectional area involving large air gaps, fringing cannot be neglected. Hence, the area is considered to be the sum of the rotor area defined by (8) and the stator area given by (10).

Finally, the inductance for each flux path is calculated using:

$$L_{ux} = \frac{N^2}{R_{gx} + R_{spx} + R_{rpx} + ½R_{syx} + ½R_{ryx}} \tag{12}$$

B. Flux Path 4

Flux path 4 is demonstrated in Figure 6.

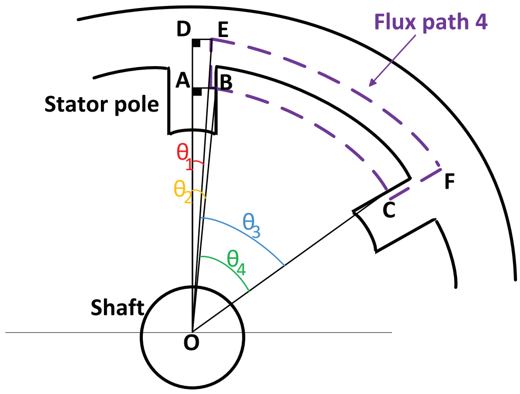

Fig. 6. Flux path 4

In this magnetic flux path, the rotor is not involved as the flux lines cross from one stator pole to the adjacent through the air gap and then returns back through the stator back iron. Hence, the three reluctances, R_{g4}, R_{sp4}, *and* R_{sy4}, could be calculated as follows:

1. Air Gap Reluctance, R_{g4}

The arc *BC* represents the average flux path length in the air gap as given by (13)

$$l_{g4}=BC=(OB)\theta_4^{rad} \tag{13}$$

The cross-sectional area is defined by:

$$A_{g4} = L\frac{h_s}{16} \tag{14}$$

2. Stator Pole Reluctance, R_{sp4}

The flux is assumed to leave the stator pole at ¾ h_s of the pole height from the top. Therefore, the average magnetic flux path length and the cross-sectional area are defined by (15) and (16), respectively for the stator pole reluctance.

$$l_{sp4} = \frac{1}{4} h_s \quad (15)$$

$$A_{sp4} = L\frac{h_s}{16} \quad (16)$$

3. Stator Back Iron Reluctance, R_{sy4}

The arc EF is the magnetic flux path length for the stator back iron reluctance, which is defined by

$$l_{sy4} = EF = (OE)\theta_3^{rad} \quad (17)$$

On the other hand, the cross-sectional area is expressed by:

$$A_{sy4} = Lb_{sy} \quad (18)$$

The flux does not link the entire number of turns per phase, N. It only links ⅜ of the turns number. Therefore, the fourth flux path inductance, L_{u4} is given by:

$$L_{u4} = \frac{(3/8 N)^2}{1/2 R_{sp4} + 1/4 R_{g4} + 1/4 R_{sy4}} \quad (19)$$

C. Flux Path 5

Figure 7 illustrates flux path 5.

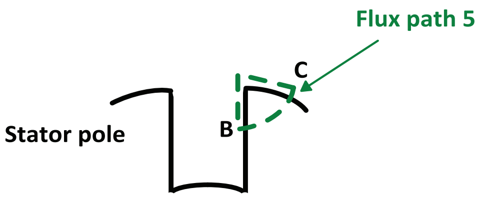

Fig. 7. Flux path 5

The flux leaves the stator pole to enter the stator back iron, passing through the air gap. The flux path is assumed to represent the perimeter of a quarter circle with center at point A and radius of a quarter the stator pole height ¼ h_s. The reluctances are calculated as follows:

1. Air Gap Reluctance, R_{g5}

The arc BC represents the length of the magnetic flux path and defined by (20). While, (21) defines the area.

$$l_{g5} = 1/2 \pi \frac{h_s}{4} \quad (20)$$

$$A_{g5} = L\frac{h_s}{16} \quad (21)$$

2. Stator Pole Reluctance, R_{sp5}

For the stator pole reluctance, the flux path length is defined by (22), and the area is expressed by (23).

$$l_{sp5} = 1/4 (h_s + b_{sy}) \quad (22)$$

$$A_{sp5} = L\frac{h_s}{16} \quad (23)$$

3. Stator Back Iron Reluctance, R_{sy5}

The mean flux path length and the cross-sectional area for the stator back iron reluctances are defined by (24) and (25), respectively.

$$l_{sy5} = \frac{1}{4} h_s \quad (24)$$

$$A_{sy5} = Lb_{sy} \quad (25)$$

The flux links only ⅛ the turns per phase N. Therefore, , which represents flux path 5 inductance is given by:

$$L_{u5} = \frac{(1/8 N)^2}{1/4 R_{sp5} + 1/4 R_{g5} + 1/4 R_{sy5}} \quad (26)$$

Finally, the effective value of unaligned inductance for the screened- SRM is calculated by summing all the flux path inductances as expressed by (27).

$$L_{ueff} = \sum_{k=1}^{5} L_{uk} \quad (27)$$

IV. SIMULATION RESULTS

In this section, the performance of the screened-SRM is investigated statically and dynamically using FEA. The static test gives an insight on the effective value of unaligned inductance to validate the proposed mathematical approach. On the other hand, the dynamic test studies the effect of varying the thickness and material of the screen on the developed torque and the current build-up process. A three-phase, 6/10 SRM with the specification in Table 1 is used for analysis.

The increased number of rotor poles allows for more space to accommodate the stator winding (since pole arcs of the new SRM are narrower than the pole arcs of a conventional three-phase SRM). According to the selected specification, the copper current density is less than $5A/mm^2$, thus special cooling is not required. For a fair comparison between unscreened and screened SRMs, the same firing angles are applied in both cases.

TABLE I. SRM SPECIFICATION

Parameter	Value
No. of phases m	3
Stator/rotor poles	6/10
Number of turns per pole N	60
Phase winding resistance R	0.8Ω
DC link voltage	500V
Rated power	6kW
Base speed	1500rpm

http://dx.doi.org/10.21622/RESD.2023.09.1.011

Axial length	240mm
Shaft diameter	40mm
Rotor outer diameter	120mm
Rotor yoke thickness	30mm
Ratio of rotor pole arc to pole pitch	0.335
Stator inner diameter	122mm
Stator outer diameter	200mm
Stator yoke thickness	25mm
Ratio of stator pole arc to pole pitch	0.21

A. Static Analysis

The proposed mathematical approach for unaligned inductance calculation is validated by a 3D FEA model. Table II shows good agreement between the proposed analytical method and the 3D FEA model.

TABLE II. UNALIGNED INDUCTANCE

Analytical	3D FEA
4.66mH	5.05mH

The inductance profile of the SRM under test is plotted in Figure 8 for both the screened and unscreened (original) SRMs.

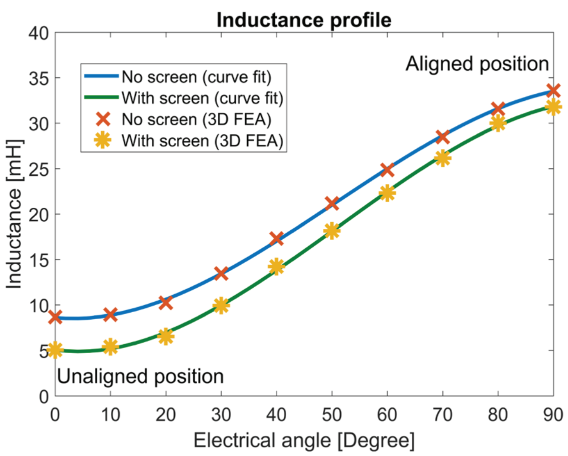

Fig. 8. Inductance profile

Results are obtained using 3D FEA model. As expected, the flux screens have insignificant effect on the aligned inductance value. On the other hand, the unaligned inductance value decreased from 8.68mH in case of unscreened SRM to reach 5.05mH for the screened SRM.

The 40% reduction in the effective unaligned inductance value will increase the conversion area (area OAB in Figure 1) resulting in more developed torque, hence increasing the torque/power density of the SRM.

B. Dynamics Analysis

The dynamic performance of the screened-SRM is presented in this sub-section using 2D FEA where the process of current build-up along with the developed torque are demonstrated. Conventional asymmetric half-bridge with two diodes and two switches per phase is used. The SRM operates in a single-pulse mode; that is, the dc-link voltage is applied for the whole dwell period. Then a negative voltage is applied at the end of the dwell period for rapid current commutation, as implied in Figure 9.

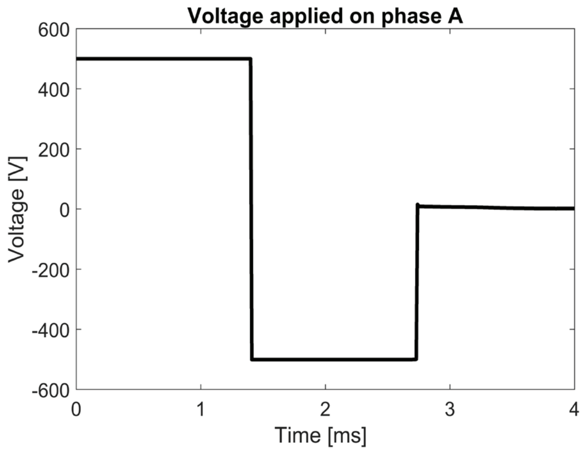

Fig. 9. The voltage applied on phase A

The dynamic performance at rated conditions is investigated, and Figure 10 compares the results of unscreened and 6mm thick Cu screened SRMs.

Figure 10a shows the phase current waveforms for the unscreened and screened SRMs. The reduction in the effective unaligned inductance alters the current response of the SRM with conducting screens. Utilizing the same dc-link voltage, the screened motor accelerates the current build-up. The rms phase current increases from 17.7A for the unscreened SRM, to 21A for the screened case. Figure 10b compares the torque profile in both cases. The screened motor is able to develop more torque as a result of a higher current and lower unaligned inductance.

The average torque of the unscreened motor is 38.6Nm. This value increases by 34% to 50.77Nm for the screened SRM, hence improving SRM torque/volume. Thus, the deployment of conducting screens improves the Nm/A by 10%, which reflects on the motor power factor [5].

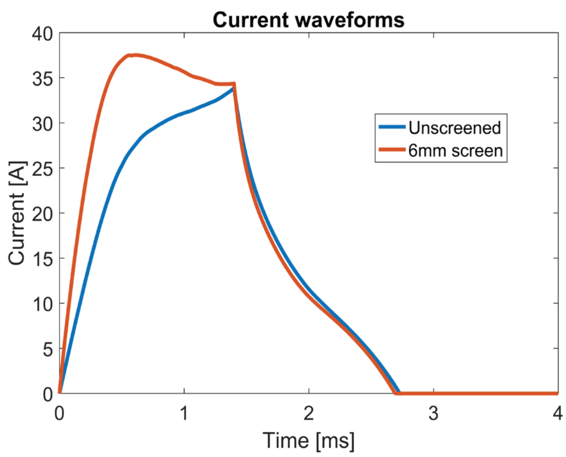

Volume 9, Issue 1, June 2023 - ISSN 2356-8569
http://dx.doi.org/10.21622/RESD.2023.09.1.011

A

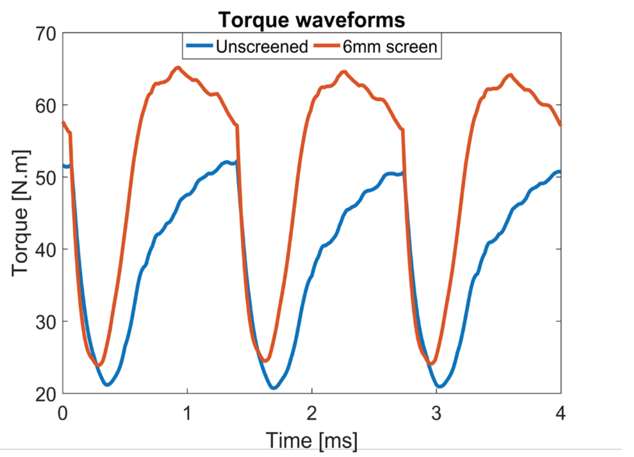

B

Fig. 10. Performance comparison of unscreened and screened SRM: (a) phase current waveforms and (b) developed torque waveforms.

Figure 11 shows the torque/speed characteristics of the unscreened and screened SRM. The screened SRM offers superior torque over the entire speed range.

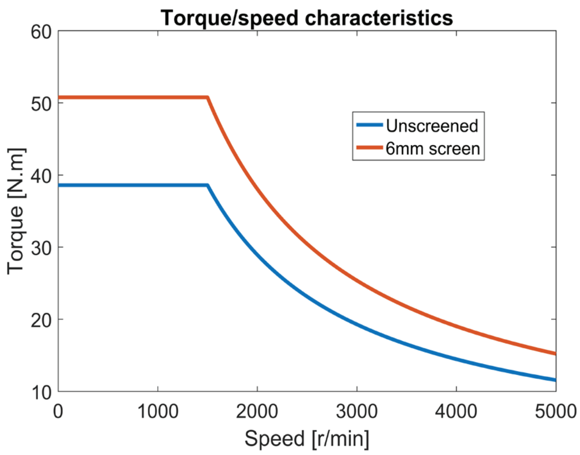

Fig. 11. Torque/speed characteristics

Below the motor base speed, current chopping control (CCC) is used. In this control technique, the motor develops its rated torque, and the speed is controlled from zero up to base speed by controlling the phase currents. Above base speed, the phase currents cannot be controlled (chopped) anymore, and the motor enters the single pulse mode. In this mode, the speed of the motor is controlled by adjusting the turn on and turn off angles. Hence, this mode is referred to as advance angle control (AAC). Above the base speed, the motor cannot produce its rated torque. However, controlling the turn on/off angles allows the motor to operate at constant power.

C. Effect of Screen Material and Thickness

This subsection investigates the screened-SRM performance when screens with different materials and thicknesses are utilized.

Figure 12 shows SRM current and torque waveforms using two different screens. The first screen is 3.5mm thick copper, while the second screen is 10 mm thick aluminum (filling the whole interpolar rotor air gaps).

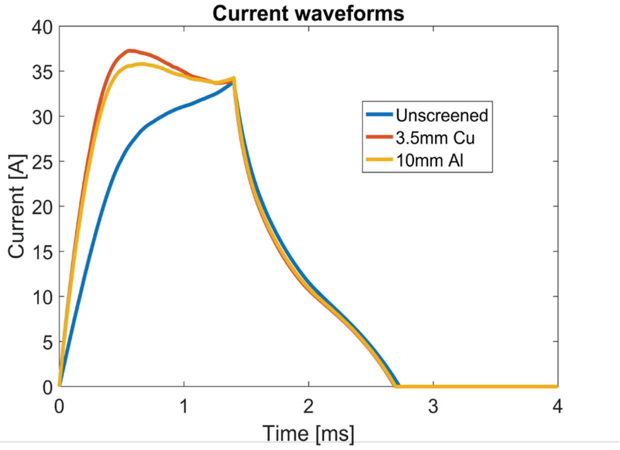

A

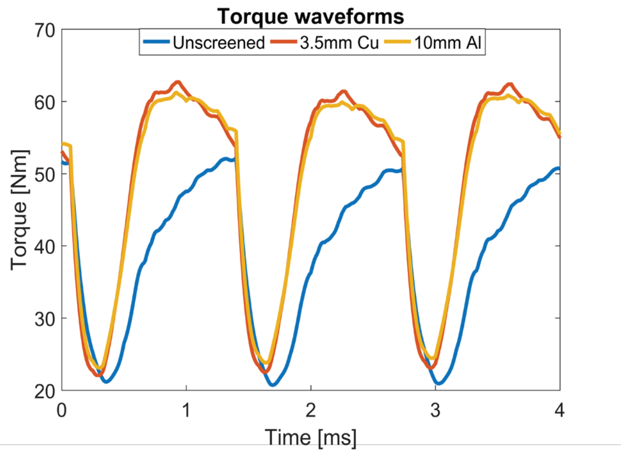

B

Fig. 12. Performance of SRM using different screen materials: (a) current waveforms and (b) torque waveforms

The electrical conductivity of copper is 5.98×10^7 *S/m* with density 8960 kg/m^3. The electrical conductivity of aluminum is 3.5×10^7 *S/m* with density 2600 kg/m^3. The SRM with a 3.5 mm copper screen is able to deliver the same output torque as the 10 mm aluminum screen. This establishes that electrical conductivity plays an important role in the behavior of the induced eddy current.

Figure 13 compares SRM performance when different thickness copper screens are deployed, where increasing the screen thickness results in more developed torque.

From this study, it is concluded that the thickness and material of the screen affect the SRM performance. Using a film screen with low conductivity results in higher resistance to the induced voltage, hence the eddy current is smaller. Increased resistivity does result in a reduced eddy current decay time constant.

Volume 9, Issue 1, June 2023 - ISSN 2356-8569
http://dx.doi.org/10.21622/RESD.2023.09.1.011

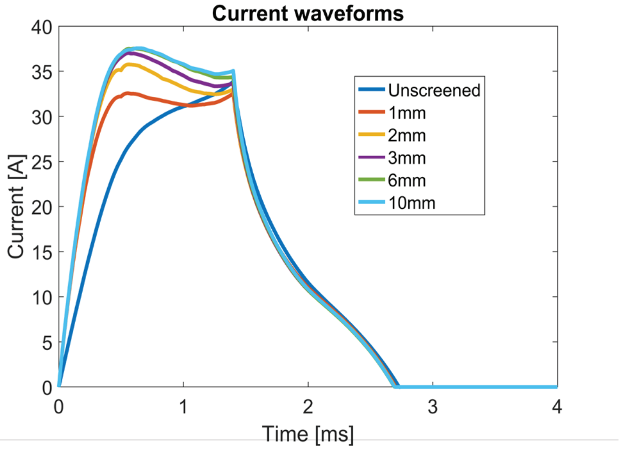

A

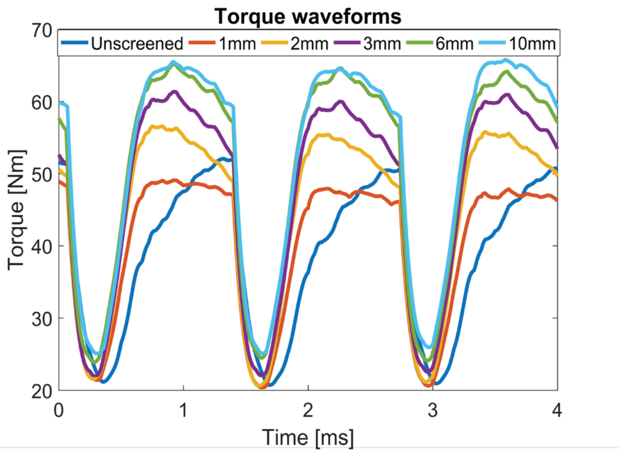

B

Fig. 13. Performance of SRM using different screen thicknesses: (a) current waveforms and (b) torque waveforms

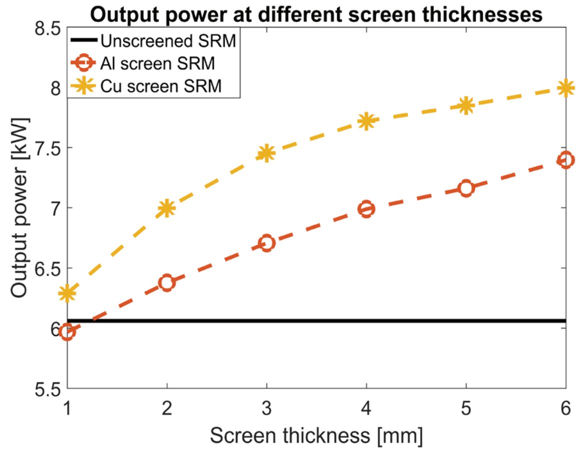

A

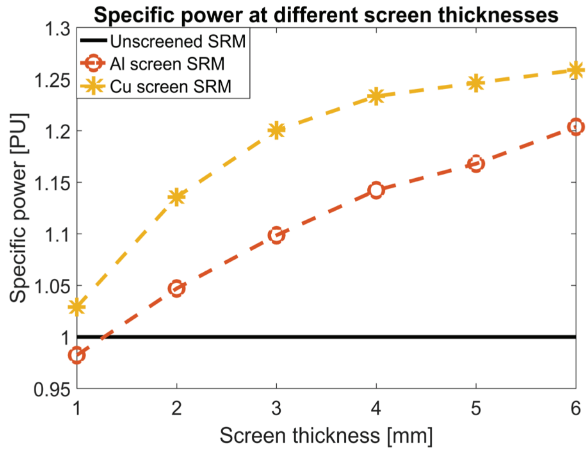

B

Fig. 14. Performance comparison of unscreened and screened SRMs: (a) output power and (b) specific power

The deployment of rotor conducting screens does not alter motor physical volume (as opposed to material volume).

Hence, the increase in output power will directly reflect the increase in power density (kW/litre), as shown in Figure 14a. The specific power (kW/kg) (which is an important factor in most applications) is compared for the unscreened and screened SRMs in Figure 14b, showing an improvement in specific power when conducting screens are used. The penalty for reducing torque ripple and improved torque and power output is screen eddy losses, which reduce machine efficiency.

VII. CONCLUSION

The paper investigated the effect of utilizing rotor conducting screens to enhance the torque capability of SRM with a higher number of rotor poles than stator poles. The rotor pole increase reduces torque ripple. However, since the interpolar rotor gaps are narrower in the new motor design, the unaligned inductance is significantly higher when compared with conventional SRM, thus reducing the conversion area. Filling the rotor interpolar gaps with electrically conducting, non-magnetic material reduces the effective unaligned inductance as a result of the opposing flux generated by eddy currents in the screens. A detailed derivation of the effective value of unaligned inductance for screened SRM was presented and validated using FEA. A 40% reduction in the unaligned inductance and a 34% increase in output torque was recorded using copper screens. Also, a 10% increase in the Nm/A, hence power factor improvement, was achieved. The effect of using conducting screens of different materials and thicknesses on SRM performance was presented. The SRM with copper screens is able to deliver more output torque. On the other hand, aluminum is lighter and cheaper. Increasing screen thickness increases torque production. Finally, screened SRMs provided better power density and specific power than unscreened SRM.

Some interesting topics could further be investigated as:

- The performance of SRM with rotor conducting screens has been reported only for motoring mode. The research could be extended to cover the generating mode.
- Given the simple coil winding arrangement in the SRM, and water cooling, advanced manufacturing techniques may offer higher copper density (slot fill factor) improvement possibilities, for example with square section conductors.

References

[1] Z. Wang, T. W. Ching, S. Huang, H. Wang, and T. Xu, "Challenges Faced by Electric Vehicle Motors and Their Solutions," IEEE Access, vol. 9, 2021, doi: 10.1109/ACCESS.2020.3045716.

[2] E. Sayed et al., "Review of Electric Machines in More-/Hybrid-/Turbo-Electric Aircraft," IEEE Transactions on Transportation Electrification, vol. 7, no. 4. 2021. doi: 10.1109/TTE.2021.3089605.

[3] L. Vadamodala et al., "Comparison of Electric Machine Types for Electrically Driven Engine Accessories Using Multiphysics Simulation Tools," IEEE Trans Ind Appl, vol. 57, no. 2, 2021, doi: 10.1109/TIA.2020.3048095.

[4] E. Bostanci, M. Moallem, A. Parsapour, and B. Fahimi, "Opportunities and Challenges of Switched Reluctance Motor Drives for Electric Propulsion: A Comparative Study," IEEE Transactions on Transportation Electrification, vol. 3, no. 1, 2017, doi: 10.1109/TTE.2017.2649883.

[5] K. M. Rahman, B. Fahimi, G. Suresh, A. V. Rajarathnam, and M. Ehsani, "Advantages of switched reluctance motor applications to EV and HEV: design and control issues," IEEE Trans Ind Appl, vol. 36, no. 1, 2000, doi: 10.1109/28.821805.

[6] A. K. Sahu, A. Emadi, and B. Bilgin, "Noise and Vibration in Switched Reluctance Motors: A Review on Structural Materials, Vibration Dampers, Acoustic Impedance, and Noise Masking Methods," IEEE Access, 2023, doi: 10.1109/access.2023.3257124.

[7] C. A. Wiguna et al., "Vibration and Acoustic Noise Reduction in Switched Reluctance Motor by Selective Radial Force Harmonics Reduction," IEEE Open Journal of Industry Applications, vol. 4, 2022, doi: 10.1109/ojia.2022.3229849.

[8] Y. Yasa, Y. Sozer, and M. Garip, "Acoustic Noise Mitigation of Switched Reluctance Machines With Leaf Springs," IEEE Transactions on Industrial Electronics, vol. 70, no. 2, 2023, doi: 10.1109/TIE.2022.3159969.

[9] A. Sohrabzadeh, H. Torkaman, and A. Y. Javid, "Improvement Undesirable Characteristics of the Switched Reluctance Motor with Triangular Rotor Structure," IEEE Transactions on Energy Conversion, pp. 1–8, 2023, doi: 10.1109/TEC.2023.3265692.

[10] K. Diao, G. Bramerdorfer, X. Sun, Z. Yang, and S. Han, "Multiobjective Design Optimization of a Novel Switched Reluctance Motor With Unequal Alternating Stator Yoke Segments," IEEE Transactions on Transportation Electrification, vol. 9, no. 1, 2023, doi: 10.1109/TTE.2022.3174337.

[11] M. Abdalmagid, M. Bakr, and A. Emadi, "A Linesearch-Based Algorithm for Topology and Generative Optimization of Switched Reluctance Machines," IEEE Transactions on Transportation Electrification, pp. 1–1, 2023, doi: 10.1109/TTE.2023.3245992.

[12] A. Chiba et al., "Torque density and efficiency improvements of a switched reluctance motor without rare-earth material for hybrid vehicles," IEEE Trans Ind Appl, vol. 47, no. 3, 2011, doi: 10.1109/TIA.2011.2125770.

[13] K. Kiyota, S. Nakano, and A. Chiba, "A Fast Calculation Method of Optimal Ratio of Outer Diameter and Axial Length for Torque Improvement in Switched Reluctance Motor," IEEE Trans Ind Appl, vol. 54, no. 6, 2018, doi: 10.1109/TIA.2018.2850024.

[14] J. W. Jiang, B. Bilgin, and A. Emadi, "Three-Phase 24/16 Switched Reluctance Machine for a Hybrid Electric Powertrain," IEEE Transactions on Transportation Electrification, vol. 3, no. 1, 2017, doi: 10.1109/TTE.2017.2664778.

[15] P. C. Desai, M. Krishnamurthy, N. Schofield, and A. Emadi, "Novel switched reluctance machine configuration with higher number of rotor poles than stator poles: Concept to implementation," in IEEE Transactions on Industrial Electronics, 2010. doi: 10.1109/TIE.2009.2034678.

[16] B. Bilgin, A. Emadi, and M. Krishnamurthy, "Design considerations for switched reluctance machines with a higher number of rotor poles," IEEE

Transactions on Industrial Electronics, vol. 59, no. 10, 2012, doi: 10.1109/TIE.2011.2141102.

[17] B. Bilgin, A. Emadi, and M. Krishnamurthy, "Comprehensive evaluation of the dynamic performance of a 6/10 SRM for traction application in PHEVs," IEEE Transactions on Industrial Electronics, vol. 60, no. 7, 2013, doi: 10.1109/TIE.2012.2196015.

[18] J. Lin, N. Schofield, and A. Emadi, "External-Rotor 6-10 Switched Reluctance Motor for an Electric Bicycle," IEEE Transactions on Transportation Electrification, vol. 1, no. 4, 2015, doi: 10.1109/TTE.2015.2502543.

[19] J. Dang, J. R. Mayor, S. A. Semidey, R. G. Harley, T. G. Habetler, and J. A. Restrepo, "Practical considerations for the design and construction of a high-speed SRM with a flux-bridge rotor," IEEE Trans Ind Appl, vol. 51, no. 6, 2015, doi: 10.1109/TIA.2015.2445813.

[20] K. Kiyota, T. Kakishima, A. Chiba, and M. A. Rahman, "Cylindrical rotor design for acoustic noise and windage loss reduction in switched reluctance motor for HEV applications," IEEE Trans Ind Appl, vol. 52, no. 1, 2016, doi: 10.1109/TIA.2015.2466558.

[21] X. Sun, K. Diao, G. Lei, Y. Guo, and J. Zhu, "Study on Segmented-Rotor Switched Reluctance Motors With Different Rotor Pole Numbers for BSG System of Hybrid Electric Vehicles," IEEE Trans Veh Technol, vol. 68, no. 6, pp. 5537–5547, Jun. 2019, doi: 10.1109/TVT.2019.2913279.

[22] Z. Xu, J. Liu, M. J. Kim, D. H. Lee, and J. W. Ahn, "Characteristics Analysis and Comparison of Conventional and Segmental Rotor Type 12/8 Switched Reluctance Motors," in IEEE Transactions on Industry Applications, 2019. doi: 10.1109/TIA.2018.2859324.

[23] B. C. Mecrow, E. A. El-Kharashi, J. W. Finch, and A. G. Jack, "Preliminary performance evaluation of switched reluctance motors with segmental rotors," IEEE Transactions on Energy Conversion, vol. 19, no. 4, 2004, doi: 10.1109/TEC.2004.837290.

[24] B. C. Mecrow, J. W. Finch, E. A. El-Kharashi, and A. G. Jack, "Switched reluctance motors with segmental rotors," IEE Proceedings - Electric Power Applications, vol. 149, no. 4, p. 245, 2002, doi: 10.1049/ip-epa:20020345.

[25] A. J. Hutton and T. J. E. Miller, "Use of flux screens in switched reluctance motors," in IEE Conference Publication, 1989.

[26] Y. G. Dessouky, B. W. Williams, and J. E. Fletcher, "Conducting screen utilisation in switched reluctance motors," IEEE Transactions on Energy Conversion, vol. 14, no. 4, pp. 946–951, 1999, doi: 10.1109/60.815012.

[27] R. Hamdy, J. E. Fletcher, B. W. Williams, and S. J. Finney, "High-speed performance improvements of a two-phase switched reluctance machine utilizing rotor-conducting screens," IEEE Transactions on Energy Conversion, vol. 17, no. 4, 2002, doi: 10.1109/TEC.2002.805202.

[28] M. M. Mahmoud, J. E. Fletcher, and B. W. Williams, "Evaluation of rotor conducting screens on the single-phase switched reluctance machine," Electric Power Components and Systems, vol. 34, no. 2, 2006, doi: 10.1080/15325000500244674.

[29] S. Xu, L. Tao, G. Han, and C. Liu, "A Novel Driven Scheme Regarding to Current Dynamics Enhancement for Switched Reluctance Motor System," IEEE Transactions on Transportation Electrification, 2023, doi: 10.1109/TTE.2023.3243176.

[30] D. Roy and M. Sengupta, "An Experimentally Validated Novel Analytical Approach for Modeling of a Saturated Switched Reluctance Motor," IEEE Trans Magn, vol. 58, no. 12, 2022, doi: 10.1109/TMAG.2022.3210155.

[31] G. Watthewaduge and B. Bilgin, "Reluctance Mesh-Based Magnetic Equivalent Circuit Modeling of Switched Reluctance Motors for Static and Dynamic Analysis," IEEE Transactions on Transportation Electrification, vol. 8, no. 2, 2022, doi: 10.1109/TTE.2021.3132885.

[32] N. K. Sheth and K. R. Rajagopal, "Calculation of the flux-linkage characteristics of a switched reluctance motor by flux tube method," IEEE Trans Magn, vol. 41, no. 10, 2005, doi: 10.1109/TMAG.2005.854865.

[33] R. Krishnan, Switched reluctance motor drives: Modeling, simulation, analysis, design, and applications. 2017. doi: 10.1201/9781420041644.

[34] P. Materu and R. Krishnan, "Analytical prediction of SRM inductance profile and steady-state average torque," in Conference Record - IAS Annual Meeting (IEEE Industry Applications Society), 1990. doi: 10.1109/ias.1990.152189.

Journal of Renewable Energy and Sustainable Development (RESD) Volume 9, Issue 1, June 2023 - ISSN 2356-8569
http://dx.doi.org/10.21622/RESD.2023.09.1.021

Received on, 04 April 2023 Accepted on, 06 June 2023 Published on, 20 June 2023

Drivers for, and barriers to solar energy use by manufacturing Micro Small and Medium Enterprises (MSMEs) in Tanzania

Felichesmi S. Lyakurwa

Mzumbe University, Department of Engineering Management Studies, Po Box 87, Mzumbe, Tanzania
Email: felichesmi.lyakurwa@mu.ac.tz

ABSTRACT

Choice of solar energy by manufacturing Micro, Small and Medium Enterprises (MSME's) has been associated with manufacturing sustainability. In this study, the Structural Equation Modeling (SEM) technique was employed to establish drivers for, and barriers to solar energy use by manufacturing MSME's in selected districts in Morogoro region. The SEM results revealed social-economic, technological and environmental factors hindering deployment of solar energy by manufacturing MSME's. Also, the results indicated that there are several factors that hinder manufacturing MSME's use of solar energy for different operations including the environmental concern (i.e., staff/employers' concern about air pollution resulted from energy use, and staff/employers' concern about climate change); solar energy awareness (i.e., experience in previous use of solar energy, and understanding of different types of solar PV which can be used at industry level), and solar energy generation cost (i.e., the generation of solar energy may cause additional cost, and solar energy requires high initial investment cost). Hence, the results of this study can be used by energy policymaking instruments to make informed decisions for renewable energy investment in the country's manufacturing sector for manufacturing sustainability.

Index-words: *Manufacturing sustainability, Renewable energy, Solar energy, SEM model*

I. INTRODUCTION

To date, there is little doubt that fossil fuels are main energy source in the global energy mix despite the highest contribution to the carbon dioxide (CO_2) concentrations in the atmosphere. In 2021, the global CO_2 emissions from energy combustion and industrial processes reached 34.9 $GtCO_2$, an increase of 4.8% from the CO_2 in 2020 (Deng & Davis, 2022). Hence, without appropriate technologies that reduce CO_2 emissions, the global average atmospheric CO_2 concentration, as well as ocean and surface temperatures, will continue to rise (Chen et al., 2022). In the world, the magnitude of CO_2 emissions varies from one sector to another whereby the industry has the highest contribution (32%), followed by building operations (28%), while transportation (23%), building materials (11%) and others contributing (6%) (Ali & Ahmad, 2020). Eleftheriadis & Anagnostopoulou (2015) documented a strong association between CO_2 emissions and rise in global temperature, and climate change. For example, Tollefson, (2021) documented that climate change impacts have increased the global surface temperature by around 1.1°C compared to average in 1850-1900, a level that has not been witnessed in the past 125000 years ago whereby the IPCC's best estimated remains at 3°C. Maximillian et al., (2019) and Yang et al., (2022) revealed that rising of the global temperature caused by Greenhouse Gases (GHG) emission has caused significant damage to the human living environment like extinction of some species, droughts, ocean acidification and sea-level rise. This has affected significantly the livelihoods of people because earning from fishing is low, reduced number of jobs, thereby leaving the community food insecure. Considering the negative social, economic and environmental effects of CO_2 emissions, many governments in the world have invested heavily on designing efficient climate change policies including emission trading schemes, carbon trading and polluter pays principle.

In spite of the short, and moderate term CO_2 emissions reduction targets can be achieved with use of such economic pricing instruments, yet ambitious emission reduction goals can be difficult to achieve without pervasive diffusion of a low-carbon technologies (Ren et al., 2021). Usually, diffusion of renewable energy sources in the national energy mix provides a basis for achieving mass reductions in CO_2 emissions in long term. For example, the European Union (EU) has set a target of 20% CO_2 emission reduction that will be achieved through consumption of more renewable energy sources (Council, 2009). Also, in 1990 the EU leaders committed about 80-95% reduction of CO_2 emissions by 2050 such that it will not be materialized unless a magnitude of 95-100% of the country's decarbonization of electricity sector is achieved (Höhne et al., 2019). According to Shahsavari & Akbari, (2018) solar photovoltaic (PV) is the most appropriate technology for a source of renewable electricity in developing countries particularly in rural areas because solar PV reduces demand for fossil fuels, and related emissions such as CO_2, nitrogen oxides (NO_x) and sulfur dioxide (SO_2). Moreover, it was projected that utilization of solar PV by production systems will reduce about 69-100 million tons of CO_2, 126,000-184,000 tons of SO_2, and 68,000-99,000 tons of NO_x by 2030 such that these reductions will decrease human exposure to serious diseases including heart attacks, and Asthma by 2030. In Tanzania, many efforts have been made to reduce CO_2 emissions, whereby reduction of CO_2 emission from cement production was reduced with replacement of fossil fuel (i.e., coal) with sawmill residues. Replacement of coal in cement production has reduced GHG emissions by 455-495 kg of CO_2eqMWh^{-1} which is equivalent to 83-91% decrease in GHG emissions (Sjølie, 2012). Also, in efforts to reduce CO_2 emissions, the government of Tanzania has invested a total of $112.4 million for renewable energy generation in the period of twelve years from 2007 to 2019 (Lyakurwa, 2022).

In the face of vast investment to ensure access, and use of renewable energy by different production sectors in the country, yet deployment of renewable energy for different applications is inadequate. Lyakurwa & Mkuna, (2018) and Elasu et al., (2023) documented several factors hindering adoption of solar energy including consumer's beliefs about renewable energy benefits, perception of self-effectiveness, political and institutional factors, environmental concern, renewable energy development and awareness, and financial abilities. According to Hasan et al., (2022) and Zulu et al., (2022), the uptake of renewable energy technologies is hindered by several factors mainly technology advancement, owner's perception, incentive policy, customer's behaviour and price of electricity that can be grouped into six groups mainly technical, economic, institutional policy, social, market and organizational. In regard to the manufacturing industries, renewable energy use for different processes is determined by different factors including socio-economic, technology, regulatory and environmental (Seetharaman et al., 2019). Based on the empirical evidence, access to clean, reliable and affordable energy for domestic and industrial uses is challenge to many developing countries of Africa that contributed greatly to dependence on the non-renewable energy mainly fossil fuels for different domestic and industrial applications. Fossil fuels are characterized with ever-increase in price, harmful effect on human health and quality of ecosystem like deterioration of aquatic lives, climate change and global warming effects.

Moreover, majority African countries including Tanzania, are blessed with renewable energy sources such as solar energy which is readily available, clean, affordable and can be used for both domestic and industrial purposes (Lyakurwa, 2022). Despite the benefits of renewable energy (i.e., solar PV), the extent to which solar energy is used for different industrial applications is low. This has brought several probing questions that tries to uncover factors hindering use of solar energy for various industrial applications. Hence this study was aimed to establish drivers for, and barriers to solar energy use by manufacturing MSME's for different industrial operations.

A. Theoretical framework

This study was guided by the theory of constraints (TOC) which has the objective of profit maximization through increased performance of a production system. Saleh et al., (2019) revealed that profit maximization can be achieved via efficient utilization, and management of all input resources e.g., energy, manpower, machine and equipment, materials, and working methods, among others. Hence, aggressive business organization places more focus on identified constrains because its elimination offers highest return towards effective and efficient resource utilization, and management. Constraint refers to as the weakest link in process of a production system whereas its improvement can be achieved through five distinct stages namely constraint identification, analysis, elevation and subordinating everything to the constraint. Application of TOC is the most appropriate strategy to solve factors hindering achievement of the goals (e.g., productivity improvement & green manufacturing) by an industry through bottlenecks identification and work out to eliminate or eradicate them. Hence, it brings benefit to industries with increased profit due to reduced production cost mainly by adoption of appropriate renewable energy technologies. In this regard, TOC can be used to establish as to why manufacturing MSME's do not use solar energy for different industrial operations. The understanding will inform formulation of strategies and policies that will promote use of solar PV by manufacturing industries for sustainable industrial development.

Kynčlová et al., (2020) sustainable industrial development refers to the situation whereby governments formulate policy and strategies that require industries to operates in a way to meet the economic objectives together with social inclusiveness and minimizing natural resource use, and environmental impacts. Usually this can be achieved with effective implementation of the United Nations Sustainable Development Goals (SDGs), preferably Goal 7: affordable and clean energy, Goal 9: industry, innovation and infrastructure, and Goal 13: climate action. The TOC therefore, is closely linked with barriers to solar energy use by manufacturing industries because they all aim at profit maximization and sustainable industrial development which can be achieved through a shift from using fossil fuels to renewable energy i.e., solar PV. Also, implementation of this theory can be achieved through application of reliable, clean and affordable energy sources by manufacturing MSME's to ensure optimal use of resources leading to less environment impacts in course of production processes. It is the interest of this study to make use of the constraint's theory to explore factors hindering manufacturing MSME's use of solar energy for manufacturing sustainability.

II. DATA AND METHODS

B. Study area

This study was conducted in the four (4) districts in Morogoro region namely Morogoro Municipal council, Mvomero district, Kilombero and Kilosa district council. Morogoro region is located at latitudes 6.8278°South of equator, and longitudes 37.6591° East of Greenwich Meridian. The region covers a total area of 70,624 Sq. Kms with a population of 2,218,492 (URT, 2013). The study was conducted in the selected districts because many households are livestock keepers and farmers whereas their produce requires value addition by manufacturing MSME's. According to Lyakurwa (2022) manufacturing enterprises are classified into four (4) broad categories based on the number of employees, total investment and sales turnover (Table 1).

TABLE I: CLASSIFICATION OF ENTERPRISES

Category	Employees	Capital investment in Machinery (TZS)
Micro enterprise	1 – 4	5 million
Small enterprise	5 – 49	>5 to 200 million
Medium enterprise	50 – 99	>200 to 800 million
Large enterprise	100+	>800 million

URT (2012)

Also, Morogoro region has adequate number of renewable energy sources including solar PV, biomass, biogas, wind and hydro power, to mention few. Despite the availability, the selected districts as other districts in Tanzania experiences inadequate access to reliable, clean and affordable energy sources whereby majority manufacturing MSME's use non-renewable energy for different applications. The dependency on non-renewable energy sources has contributed greatly to the regions' failure to realize the Tanzania National Five-Year Development Plan 2021/22 - 2025/26, National Strategy for Growth and Reduction of Poverty (NSGRP), the SGDs, and the Tanzania Development Vision 2025 (URT, 2000; URT, 2010; URT, 2021; Sonter & Kemp, 20212015). Hence, developing barriers to solar energy use by manufacturing MSME's is critical towards achievement of the SDGs, NSGRP, Tanzania vision 2025 and National Five-Year Development Plan of 2021/22 to 2025/26.

C. Research design, data sources, and collection process

A cross sectional survey research design was employed to establish barriers to solar energy use by the manufacturing MSMEs in the selected four (4) districts in Morogoro region. According to Van der Stede (2014), this design enables collection of large amounts of data at one location in time in the most economical way. The method was also supported by Connelly (2016) which documented that, a cross sectional survey design is mostly appropriate when the study intends to answer questions of who, what type, where, how many and how much as revealed by this study. A well-structured questionnaire and interviews guide questions were used to collect primary data from the manufacturing MSME's located in Morogoro Municipal council, Mvomero, Kilombero and Kilosa district councils. The multistage sampling technique was applied in the selection of representative manufacturing MSME's (i.e., a sample size *(n)* of 242 enterprises) in the selected districts.

D. Methods for data analysis

The preliminary, descriptive and inferential statistical analysis methods were employed in the analysis of the collected data about workers perceptions about sustainable manufacturing practices as well as drivers for, and barriers to solar energy use by the manufacturing MSME's in the selected districts in Morogoro region. Preliminary analysis involved data quality check and testing the assumptions of Exploratory Factors Analysis (EFA) such that all missing values were checked. The normality of data was also checked to establish whether the collected data are good for the Structural Equation Modeling (SEM) through Confirmatory Factor Analysis (CFA). Thereafter, the descriptive and inferential analysis were carried out. The descriptive analysis was conducted to different data groups mainly gender, work experience, education level, number of employees, and capital invested in the business, among others. The descriptive analysis intended to provide an insight of some findings, which may not necessarily be in the focus of the study's specific objectives. The inferential analysis i.e., EFA and CFA were performed.

The EFA was conducted in each construct (i.e., Environmental Concern (Ec), Solar Energy Awareness (sea), Self-Effectiveness Perception (sep), Solar Energy Generation Cost (segc), Solar Technology Advancement (sta), Perceived Benefits of Solar Energy (pb), MSME's Intention to Use Solar Energy (msme'siuse), and Risk/Trust Perception of Solar Energy (rtse)), and confirm variables in different groups of the factors hindering use of solar energy by manufacturing MSME's. The SEM through CFA has been applied in modeling drivers for adoption of manufacturing technologies and renewable power generation (Hariyani & Mishra, 2023; Jabeen et al., 2019), and barriers to sustainable construction and sweetened beverages consumption (Durdyev et al., 2018; Wang & Chen, 2022). The confirmed factors were analyzed by using CFA so as to identify the relative importance of each towards deployment of solar energy by manufacturing enterprises. Thereafter, the inferential analysis mainly correlation analysis was used to characterize the relationship between the variables i.e., factors influencing decision to use solar energy by manufacturing MSME's.

III. RESULTS AND DISCUSSION

E. Respondents profile

Table II presents the descriptive statistics of the respondent characteristics for drivers for, and barriers to solar energy use by manufacturing MSME's in Tanzania.

http://dx.doi.org/10.21622/RESD.2023.09.1.021

TABLE II: RESPONDENT PROFILE

S/No.	Variable measure	N	%
Gender	Male	166	72
	Female	66	28
Age	18-24	37	16
	25-31	83	35
	32-38	81	34
	>39	35	15
Work experience	1-5	91	42
	6-10	78	36
	11-15	19	9
	16-20	19	9
	>20	11	5
Marital status	Married	86	49
	Single	91	51
Workers education	Primary	13	6
	Secondary	112	50
	Degree	98	44

The results (Table II) indicate that out of 232 staff working in the manufacturing MSME's, 166(72%) were male and 66(28%) were female which implies that tasks performed by these industries are not masculine and a sign of gender balanced working environment. In regard to the workers age, 38(17%) have ages ranging 18-24 years, 83(35%) ages 25-31 years, 80(34%) ages 32-38 years, while 35(15%) aged more than 39 years old. The results imply that majority working staff are young, matured and energetic person that reflects empowerment of youths. The results for the working experience showed that majoring staff are new employees with working experience ranging 1-5 years, that is 91(42%), followed by a working experience of 6-10 years i.e., 78(36%), while the manufacturing MSME's have few staff with a working experience more than 20 years, that is 11(5.0). Considering the workers education level, majority have secondary education, 112(50%), followed by degree holders, a total of 98(44%), and 13(6%) have a primary education. The results imply that the surveyed manufacturing MSME's have employed staff trained at different levels to work in different production sectors.

F. Drivers for, and barriers to solar energy use by manufacturing MSME's

The CFA revealed seven (7) factors that drive manufacturing MSMEs' deployment of solar energy in different operations. With the CFA, it was assumed that there would be a single dominant factor whereas a number of factors were specified whereas the covariance of the 7 factors are fully explained by the single latent variable plus the unique variance of each factor. In this case, the unique variance or error variance, is being estimated for each of the seven (7) observed indicator variables (Figure 1). In the CFA, it was assumed that deployment of solar energy by a manufacturing MSMEs' should explain all the variance among seven factors. At first place, weak results were obtained such that stronger results will be obtained by removal of the measurement error given the latent variables are subsequently used as independent or dependent variables in a SEM. The CFA model was fitted by using a maximum likelihood estimation method whereby variance-covariance matrix of the estimators i.e., the standard errors were computed using an observed information matrix. Usually, with the assumption of normality, this method is often the best option and is fairly robust even with same violation of normality since it uses a listwise deletion approach (Lee et al., 2002).

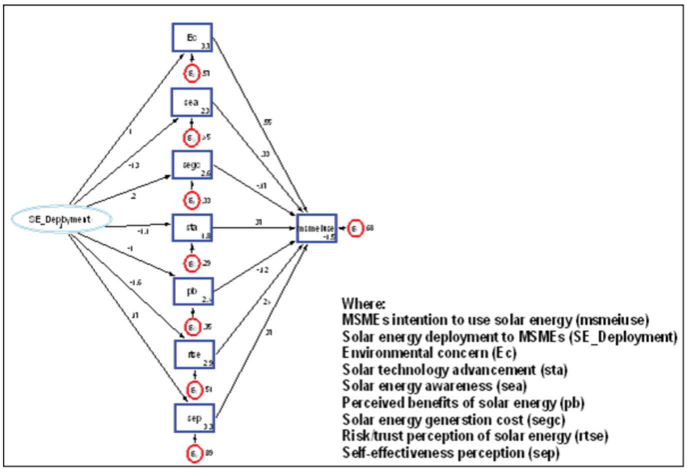

Figure 1: CFA Model for drivers to the solar energy use by MSMEs'

Figure 1 is the path diagram for a SEM model with observed exogeneous variables and a latent variable. The model can be represented with a mathematical notation by a general equation 1 as follows:

$$Y_i=\beta_{i0}+M+\beta_{1i}X_i+\ \dots\ +B_{in}X_n+\epsilon_i;\ given\ i=1,\dots,n \qquad (1)$$

where,

$(Y,X_1,\dots,X_n)$~iid with mean μ and covariance matrix Σ;

$$\epsilon=(\varepsilon_1,\varepsilon_2,\varepsilon_3)',E(\epsilon)=(0,0,0)',var(\epsilon)=\begin{bmatrix}\sigma_1^2 & 0 & 0\\ 0 & \sigma_2^2 & 0\\ 0 & 0 & \sigma_3^2\end{bmatrix},E(M)=0,\text{ and } var(M)=\sigma_M^2;var(M)=\sigma_M^2$$

Y is the dependent exogeneous variable (MSMEs intention to use solar energy);

Xs are the independent observed exogeneous variables; and

M is the single latent variable i.e., Deployment of Solar energy to MSMEs.

Fitting the CFA model

The Comparative Fit Index (CFI) and Tucker Lewis Index (TLI) are both incremental fit indices values >0.95 whereby these indices indicate a very good fit (Sahoo, 2019) structural equation modeling is a buzz word in the arena of research in management, social sciences, and other equivalent fields. Although the theoretical base bears its significance in building the measurement and structural models, assessing different goodness-of-fit indices (GOFI. Shi et al., (2019)the Tucker–Lewis index (TLI indicated that values from 0.90 or above are considered evidence of the acceptable model fit. Also, the Standardized Room Mean Square Residual (SRMR) values up to 0.05 are considered

 Volume 9, Issue 1, June 2023 - ISSN 2356-8569
http://dx.doi.org/10.21622/RESD.2023.09.1.021

indicative of a close-fitting model whereas the values ranging between 0.05 up to 0.10 suggest acceptable fit. The SEM model fitting results presented in Table III showed that, the CFI (0.348) and TLI (0.088) values are lower than 0.90. Thus, the CFI and TLI indicates poor model fitting such that re-analysis was performed to generate standardized results.

TABLE III: SEM MODEL FITTING RESULTS

Fit statistic	Value	Description
Likelihood ration		
Chi2ms(20)	235.501	model vs. saturated
p>chi2	0.000	
p>bs(28)	358.757	baseline vs. saturated
p>chi2	0.000	
Population error		
RMSEA	0.221	Root mean square error of approximation
90% CI, lower bound	0.196	
upper bound	0.247	
pclose	0.000	Probability RMSEA<=0.05
Information ccriteria		
AIC	3950.776	Akaike's information criteria
BIC	4032.332	Bayesian information criteria
Baseline comparisonn		
CFI	0.348	Comparative fit index
TLI	0.088	Tucker-Lewis index
Size of residuals		
SRMR	0.166	Standard root mean squared residual
CD	1.000	Coefficient of determinationn

CFA model estimation and interpretation

Table IV indicates that there are 21 observations with missing values excluded in the model because the default estimation method i.e., maximum likelihood uses listwise deletion such that all observations which do not have a response for all factors are dropped off (Chen et al., 2020)whereas the model of interest to the researcher is at the composite (scale score. All observed factors from Environmental Concern (ec) to Self-Effectiveness Perception (sep) in the model are all endogenous variables i.e., these measurement variables depend on the latent variable i.e., the Solar Energy Deployment (SE-Deployment). Also, the maximum likelihood estimator maximizes the log-likelihood function such that with the listwise deletion method, only 221 observations were available with no missing values. The results present the "Measurement" and a "Variance". The measurement gives estimates of unstandardized measurement coefficients i.e., factor loadings, their standard errors, and a z-test for each estimate along loadings. To identify the variance of the latent variable, (i.e., Solar Energy Deployment), the software fixes the loading of the first indicator at 1.0 that is called, a reference indicator whereas all unstandardized estimates will change if there is a change in reference indicator.

TABLE IV: CFA MODEL ESTIMATION AND INTERPRETATION

Structural equation model
Estimation method = ml   Number of observations = 221
Log Likelihood = -1617.7867
(1) Ec [SE_Deployment] = 1

Measurement	Coef.	Std. Err.	z	p>IzI	[95% Conf. Interval]	
Ec						
SE_Deployment	.1671627	.0772	2.17	0.030	.0158534	.318472
Const.	4.902182	.2426813	20.20	0.000	4.426535	5.377829
sea						
SE_Deployment	-.6727413	.0789552	-8.62	0.000	-.8257267	-.5197558
Const.	2.911463	.1539569	18.91	0.000	2.609713	3.213213
segc						
SE_Deployment	.3142185	0.0731089	4.30	0.000	.1709278	.4575093
Const.	4.399605	.2198134	20.02	0.000	3.968779	4.830432
sta						
SE_Deployment	-.7953117	.0839691	-9.47	0.000	-.9598881	-.6307354
Const.	2.750931	01471264	18.70	0.000	2.462568	3.039293
pb						
SE_Deployment	-.2359973	.0764013	-3.09	0.002	-.3857411	-.0862535
Const.	4.10418	.2064804	19.88	0.000	3.699486	4.508874
rtse						

http://dx.doi.org/10.21622/RESD.2023.09.1.021

Structural equation model
Estimation method = ml Number of observations = 221
Log Likelihood = -1617.7867
(1) Ec [SE_Deployment] = 1

Measurement	Coef.	Std. Err.	z	p>IzI	[95% Conf. Interval]	
SE_Deployment	-.2337238	.0867011	-3.01	0.003	-.3859403	-.0815072
Const.	3.926254	.1984981	19.78	0.000	3.537205	4.315303
sep						
SE_Deployment	.2292345	.0867011	2.64	0.008	.0593035	.3991654
Const.	3.618576	.1847959	19.58	0.000	3.256383	3.980769

The CFA results revealed that, three factor loadings (i.e., msmeiuse (p_{value}=0.030), rtse (p_{value}=0.039) and sep (p_{value}=0.001)) are statistically significant (all p_{value} < 0.050). This is construed to mean that such the indicator variables (MSME's intention to use solar energy (msmeiuse), Risk Perception of Solar Energy (rtse), and Self-Effectiveness Perception (sep)) are significantly related to their respective factors, and therefore the main drivers for the solar energy use by manufacturing MSME's in Tanzania. The results are in-line with the study by Schoeneberger et al., (2020) which explored drivers for deployment of solar PV by manufacturing industries in US whereby economic, environmental and technological factors were critical for solar PV deployment.

G. Barriers to solar energy use by manufacturing MSME's

Factor hindering manufacturing MSMEs' use of solar energy for different activities are explained by eight (8) constructs i.e., Environmental Concern (Ec), Solar Energy Awareness (sea), Solar Energy Generation Cost (segc), Solar Technology Advancement (sta), Perceived Benefits of Solar energy (pb), MSME's Intention to Use Solar Energy (msme'siuse), Risk/Trust Perception of Solar Energy (rtse)), and Self-Effectiveness Perception (sep). The correlation results (Table V) showed that factors hindering solar energy use by manufacturing MSMEs' are environmental concern (positive correlation=0.2070), segc (positive correlation=0.0726) and sep (positive correlation=0.0816), while the factors such as sta (-0.1195), pb (-0.0123), msme'siuse (-0.067) and rtse (-0.0477) have negative correlation.

TABLE V: CORRELATION ANALYSIS

	Factors	Ec	sea	segc	sta	pb	msmeiuse	rtse
Factors	1							
Ec	0.2070	1						
sea	-0.0255	-0.0572	1					
segc	0.0726	-0.0244	-0.1975	1				
sta	-0.1195	-0.1579	0.5321	0.29	1			
pb	-0.0123	0.079	0.1071	0.02	0.2074	1		
msmeiuse	-0.067	0.4052	0.3094	0.13	0.3091	0.118	1	
rtse	-0.0477	-0.0709	0.193	0.18	0.1742	0.4428	0.2007	1
sep	0.0816	0.2966	-0.2565	0.18	-0.112	0.0355	0.325	0.0855

CFA of factors hindering use of solar energy by manufacturing MSMEs'

The exploratory factor analysis (EFA) was conducted in each construct by using the Principal Component Factor method which involved several processes including data examination, factor analysis, rotation and prediction of values. The examined data are presented in Table VI.

TABLE VI: DATA EXAMINATION

Variable	Obs.	Unique	Mean	Min	Max	Label
Ec	233	18	3.682	1.60	5.00	Environmental concern
sea	236	18	2.374	1.00	5.00	Solar Energy Awareness
segc	241	13	2.585	1.00	4.00	Solar Energy Generation Cost
sta	236	13	1.894	1.00	5.00	Solar Technology Advancement
pb	241	15	2.466	1.00	5.00	Public Benefits of Solar Energy
msmeiuse	240	17	3.156	1.00	5.00	MSME's Intention to Solar Energy
rtse	237	16	2.889	1.00	5.00	Risk Perception of Solar energy
sep	240	16	3.256	1.00	5.00	Self-Effectiveness Perception

The examination results (Table VI) revealed that there were eight constructs whereas their mean values range from 1.894 to 3.6815.

The factor analysis revealed eight principle factors with eigen values, and proportions as indicated in Table VII.

TABLE VII: FACTOR ANALYSIS RESULTS

Factor analysis/correlation			number of obs=221	
Methods: Principal-component factors			retained factors=3	
Rotation:(unrotated)			number of params=21	
Factor	Eigenvalues	Differences	Proportion	Cumulative
Factor1	2.10884	0.37864	0.2636	0.2636
Factor2	1.73019	0.34917	0.2163	0.4799
Factor3	1.38103	0.55016	0.1726	0.6525
Factor4	0.83087	0.11617	0.1039	0.7564
Factor5	0.7147	0.18972	0.0893	0.8457
Factor6	0.52497	0.15444	0.0656	0.9113
Factor7	0.37054	0.03167	0.0463	0.9576
Factor8	0.33887		0.0424	1
LR test: independent vs. saturated: chi2(28) = 353.08 Prob>chi2=0.000				
Factor loadings (pattern matrix) and unique variances				
Variables	Factor1	Factor2	Factor3	Uniqueness
Ec	0.0705	0.6788	-0.4300	0.3494
sea	0.7418	-0.3022	-0.1044	0.3475
segc	-0.333	0.3354	0.5737	0.4476
sta	0.775	-0.2775	-0.0822	0.3157
pb	0.4744	0.2283	0.5257	0.4465
msmeiuse	0.6122	0.5200	-0.3535	0.2299
rtse	0.4893	0.2419	0.6660	0.2585
sep	-0.0538	0.7795	-0.0669	0.3850

The eigenvalues explain factors in terms of variability such that only three components i.e., Ec, sea, segc were retained because their eigenvalues are greater than 1 (Table VII). This indicates that the main factors hindering manufacturing MSMEs' use of solar energy falls in the three constructs i.e., environmental concern (Ec): staff/employers' concern about air pollution resulted from energy use, staff/employers' concern about climate change, staff/employer concern about source of energy which do not deteriorate the quality of ecosystem – biodiversity, decline of animal species, staff/employer's concern on water/land pollution caused by energy use by MSME's and staff/employer's concern about waste reduction); solar energy awareness (sea): Experience in previous use of solar energy, awareness of solar PV use and needs/benefits, understanding of different types of solar PV which can be used at industry, availability of technical solutions for solar PV and awareness of the benefits-costs of solar PV; and solar energy generation cost (segc): The generation of solar energy may cause additional cost, Solar energy requires high initial investment cost, Solar energy consumption needs a high Set-up & installation cost, and Solar PV systems requires high repair cost. These results are in-line with Lowe & Drummond, (2022) high rates of growth appear likely to continue. In this paper we use 'top-down' extrapolation of global trends and simple and transparent models to attempt to falsify the proposition that PV and wind have the potential to achieve dominance in global primary energy supply by 2050. We project future deployment of PV and wind using a logistic substitution model, and examine a series of potentially fundamental constraints that could inhibit continued growth. Adopting conservative assumptions, we find no insuperable constraints across physical and raw materials requirements, manufacturing capacity, energy balance (EROEI study about global wind and solar energy supply, which revealed that use of renewable energy for different industrial purposes is hindered by various social (e.g., health impacts of the energy use for different industrial purposes), economic (e.g., high investment cost), and environmental (e.g., emission of GHGs) factors. These barriers to solar energy use not only resulted into social, economic and environmental problems but also delayed the growth and development of the manufacturing sector in Tanzania.

For example, Rocco et al., (2020)together with a low electrification rate, are a limitation to growth, this paper studies the implications on the country's sustainable development of expanding the electricity sector. The analysis is based on the joint use of the OSeMOSYS open-source power system optimization model and the Leontief Input-Output model (based on the Tanzanian Social Accounting Matrix found that lack of infrastructure for hydro-electric generation is the main cause of low electrification rate and ultimately has limited the growth of manufacturing sector in the country. With the industrialization strategy in Tanzania access to clean, affordable and reliable energy source is critical since it the only way manufacturing industries can improve its operational performance i.e., ensure quality products, reduced cost of production and idle time, increase productivity, and achieve production flexibility. These will ensure a competitive position of the manufacturing MSME's in the local and international markets due to low production cost and ability to set a competitive selling price as well as compliance to the global standards like assurance of environmental performance of manufactured after use e.g., eco-labelling. In addition, the proportions explain the contribution of each factor in the model whereby factor1 (i.e., environmental concern) contribute about 26.36% of the total variance, which is the strongest factor. Also, uniqueness explains the percentage of variance for the factor that is not explained by the common factors. Also, Table VII revealed that all values are not greater than 0.6 which implies that these values are considered low. Therefore, the higher the uniqueness, the more likely that it is more than just a measurement error. Factor rotation maintains that factor 1 (i.e., the environmental concern) is the strongest factor with a proportion of 25% (Table VIII.

TABLE VIII: FACTOR ROTATION

Factor analysis/correlation			Number of obs = 221	
Method: Principal-component factors			Retained factors = 3	
Rotation: Orthogonal varimax (Kaiser off)			Number of params = 21	
Factor	Variances	Difference	Proportion	Cumulative
Factor1	1.9705	0.28614	0.2463	0.2463
Factor2	1.68436	0.11915	0.2105	0.4569
Factor3	1.56521		1957	0.6525
LR test: independent vs. saturated: chi2(28) = 353.08, Prob>chi2=0.000				
Rotated factor loadings (pattern matrix) and unique variances				
Variable	Factor1	Factor2	Factor3	Uniqueness
Ec	-0.0918	0.7921	-0.1214	0.3494
sea	0.7915	-0.02	0.1602	0.3475
segc	-0.6041	-0.0579	0.4292	0.4476
sta	0.8024	-0.0004	0.2014	0.3157
pb	0.1433	0.0803	0.7256	0.4465
msmeiuse	0.4124	0.7615	0.142	0.2299
rtse	0.1064	0.0325	0.8539	0.2585
sep	-0.3535	0.6825	0.1559	0.385
Factor rotation matrix				
	Factor1	Factor2	Factor3	
Factor1	0.8513	0.2577	0.4571	
Factor2	-0.4215	0.8546	0.3033	
Factor3	-0.3125	-0.4509	0.8361	

Table IX presents the predicted values based on the varimax rotated loadings of the variables by a regression method.

TABLE IX PRINCIPLE COMPONENT PREDICTED VALUES

Predict factor 1, factor 2, factor 3 (regression scoring assumed) Scoring coefficients (method=regression; based on varimax rotated factors)			
Variables	Factor1	Factor2	Factor3
Ec	0.03963	0.48426	-0.12607
sea	0.3967	0.02452	0.04462
segc	0.34591	0.06233	0.33393
sta	0.39903	0.01556	0.06958
pb	0.01692	0.00092	0.46113
msmeiuse	0.20042	0.44704	0.00984
rtse	0.01211	0.03818	0.55167
sep	0.19649	0.4003	0.08449

The results (Table X) revealed that the mean score regarding factors hindering manufacturing MSMEs' use of solar energy to be 2.79, and a standard deviation of 0.38. Also, the means score of the factors hindering solar energy deployment revealed a normal distribution curve (Figure 2).

TABLE X: MEAN SCORE OF THE FACTORS HINDERING USE OF SOLAR ENERGY

Summarize: SE_Deployment, detail				
SE_Deployment				
	Percentiles	Smallest		
1%	1.94375	1.541667		
5%	2.270833	1.57619		
10%	2.43125	1.94375	obs	242
25%	2.535417	1.972917	Sum of wgt	242
50%	2.7125		Mean	2.786757
		largest	Std. Dev	0.3818454
75%	3.04375	3.7125		
90%	3.30625	3.7125	variance	0.1458059
95%	3.40000	3.7125	skewness	0.2019058
99%	3.71250	3.8750	kurtosis	3.365797

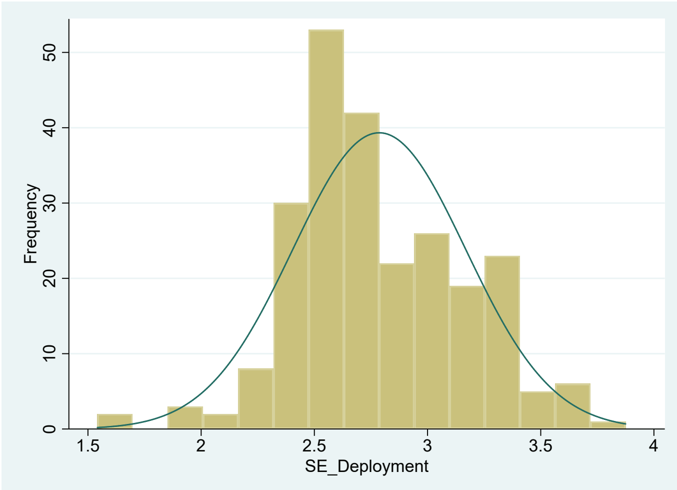

Figure 2: Distribution of factors hindering solar energy

IV. CONCLUSION

The main objective of this study was to determine drivers for, and barriers to solar energy use by manufacturing MSME's in the selected districts in Morogoro region. As the first study to model drivers for, and barriers to solar energy use by manufacturing MSME's in Tanzania, the main drivers for solar energy use were established by using the SEM. The results revealed that drivers for manufacturing MSME's deployment of solar energy for different operations includes the environmental concern, solar energy awareness, energy generation cost, technological advancement, benefits of solar use, and risk perceptions. In this regard, manufacturing MSME's management have significant influence on deployment of solar energy for different industrial operations. For example, the extent to which top management and

http://dx.doi.org/10.21622/RESD.2023.09.1.021

leaders, are exposed to the cost and benefits of renewable energy, determines decisions made for solar energy use, and even approve education programme to the staff about renewable energy technologies. In addition, SEM results indicates that there are three main factors that hinder deployment of solar energy by manufacturing MSME's including environmental concern, solar energy awareness, and solar energy generation cost.

As far as solar energy generation cost is one of the factors hindering MSME's deployment of solar energy, effective policy could involve offering tax subsidy to renewable energy production facilities i.e., machines and equipment; together with enforcement of National Environmental Management Act of Tanzania and its regulations like the sub-section which states about "polluter pays principle" for industries to strictly use energy sources that are environmentally friendly. The SEM results therefore, provides critical information to energy policymaking instruments in Tanzania about drivers for and barriers to solar energy deployment by manufacturing MSME's and make informed decisions about renewable energy technologies to be considered for investment in Tanzania.

ACKNOWLEDGEMENTS

This study was supported by VLIR-UOS Project 3, Mzumbe University, Tanzania.

REFERENCES

[1] K. A. Ali, M. I. Ahmad, and Y. Yusup, "Issues, impacts, and mitigations of carbon dioxide emissions in the building sector," *Sustainability (Switzerland)*, vol. 12, no. 18, 2020, doi: 10.3390/SU12187427.

[2] L. Chen, V. Savalei, and M. Rhemtulla, "Two-stage maximum likelihood approach for item-level missing data in regression," *Behav Res Methods*, vol. 52, no. 6, 2020, doi: 10.3758/s13428-020-01355-x.

[3] L. M. Connelly, "Cross-Sectional Survey Research," *MEDSURG Nursing Journal*, vol. 25, no. 5, p. 369, 2016.

[4] "Directive 2009/28/EC of the European Parliament and of the Council of 23 April 2009 on the promotion of the use of energy from renewable sources and amending and subsequently repealing Directives 2001/77/EC and 2003/30/EC ," *Official Journal of the European Union*, vol. L 140, no. 16, pp. 16–42, 2009.

[5] Z. Liu, Z. Deng, S. J. Davis, C. Giron, and P. Ciais, "Monitoring global carbon emissions in 2021," *Nat Rev Earth Environ*, vol. 3, no. 4, pp. 217–219, Mar. 2022, doi: 10.1038/s43017-022-00285-w.

[6] J. Elasu, J. M. Ntayi, M. S. Adaramola, and F. Buyinza, "Drivers of household transition to clean energy fuels: A systematic review of evidence," *Renewable and Sustainable Energy Transition*, vol. 3, 2023, doi: 10.1016/j.rset.2023.100047.

[7] I. M. Eleftheriadis and E. G. Anagnostopoulou, "Identifying barriers in the diffusion of renewable energy sources," *Energy Policy*, vol. 80, 2015, doi: 10.1016/j.enpol.2015.01.039.

[8] A. S. M. M. Hasan, M. A. Kabir, M. T. Hoq, M. T. Johansson, and P. Thollander, "Drivers and barriers to the implementation of biogas technologies in Bangladesh," *Biofuels*, vol. 13, no. 5, 2022, doi: 10.1080/17597269.2020.1841362.

[9] Niklas Höhne *et al.*, *A possible 2050 climate target for the EU*. Cologne: NewClimate Institute, 2019. [Online]. Available: https://newclimate.org/sites/default/files/2019/09/EU2050_Target_Adequacy.pdf

[10] C. L. O. Peters and C. Enders, "A primer for the estimation of structural equation models in the presence of missing data: Maximum likelihood algorithms," *Journal of Targeting, Measurement and Analysis for Marketing*, vol. 11, no. 1, 2002, doi: 10.1057/palgrave.jt.5740069.

[11] R. J. Lowe and P. Drummond, "Solar, wind and logistic substitution in global energy supply to 2050 – Barriers and implications," *Renewable and Sustainable Energy Reviews*, vol. 153. 2022. doi: 10.1016/j.rser.2021.111720.

[12] F. S. Lyakurwa, "Achieving Sustainability in Manufacturing Micro, Small and Medium Enterprises (MSMEs') in Tanzania Through Adoption of Solar Energy," *Journal of Industrial Engineering and Halal Industries*, vol. 3, no. 2, pp. 77–89, 2022, doi: doi.org/10.14421/jiehis.3853.

[13] F. S. Lyakurwa and E. Mkuna, "Political-institutional barriers to energy access and efficiency in Tanzania: a case study of Mvomero District," *Afrika Focus*, vol. 31, no. 1, 2018, doi: 10.21825/af.v31i1.9045.

[14] L. Ren, S. Zhou, T. Peng, and X. Ou, "A review of CO2 emissions reduction technologies and low-carbon development in the iron and steel industry focusing on China," *Renewable and Sustainable Energy Reviews*, vol. 143, p. 110846, Jun. 2021, doi: 10.1016/j.rser.2021.110846.

[15] *Tanzania in Figures 2012*. National Bureau of Statistics Ministry of Finance, 2013. [Online]. Available: https://www.nbs.go.tz/nbs/takwimu/references/Tanzania_in_figures2012.pdf

[16] M. Sahoo, "Structural Equation Modeling: Threshold Criteria for Assessing Model Fit," in *Methodological Issues in Management Research: Advances, Challenges, and the Way Ahead*, 2019. doi: 10.1108/978-1-78973-973-220191016.

[17] C. Saleh, T. Immawan, A. B. Hassan, and M. N. Zakka, "Profit Optimization Through the Application of Theory of Constraints (TOC): A Case Study in Printing Company," in *IOP Conference Series: Materials Science and Engineering*, 2019. doi: 10.1088/1757-899X/530/1/012045.

[18] C. A. Schoeneberger, C. A. McMillan, P. Kurup,

S. Akar, R. Margolis, and E. Masanet, “Solar for industrial process heat: A review of technologies, analysis approaches, and potential applications in the United States,” *Energy*, vol. 206. 2020. doi: 10.1016/j.energy.2020.118083.

[19] Seetharaman, K. Moorthy, N. Patwa, Saravanan, and Y. Gupta, “Breaking barriers in deployment of renewable energy,” *Heliyon*, vol. 5, no. 1, 2019, doi: 10.1016/j.heliyon.2019.e01166.

[20] D. Shi, T. Lee, and A. Maydeu-Olivares, “Understanding the Model Size Effect on SEM Fit Indices,” *Educ Psychol Meas*, vol. 79, no. 2, 2019, doi: 10.1177/0013164418783530.

[21] H. K. Sjølie, “Reducing greenhouse gas emissions from households and industry by the use of charcoal from sawmill residues in Tanzania,” *J Clean Prod*, vol. 27, 2012, doi: 10.1016/j.jclepro.2012.01.008.

[22] L. J. Sonter and S. Kemp, “Connecting the UNESCO Sustainable Development Goals with Australian Early Childhood Education Policy to Transform Practice,” *International Journal of Early Childhood Environmental Education*, vol. 9, no. 1, 2021.

[23] U. R. of Tanzania, “National Strategy for Growth and Reduction of Poverty II: NSGRP II,” *Ministry of Finance and Economic Affairs Tanzania*, no. July, 2010.

[24] J. Tollefson, “IPCC climate report: Earth is warmer than it’s been in 125,000 years,” *Nature*, vol. 596, no. 7871, 2021, doi: 10.1038/d41586-021-02179-1.

[25] URT, “The Tanzania Development Vision 2025,” *Ministry of Planning*. 2000.

[26] URT, “National Five Year Development Plan 2021/22-2025/26: Realising Competitiveness and Industrialisation for Human Development,” *The United Republic of Tanzania*, no. June, 2021.

[27] W. A. Van der Stede, “A manipulationist view of causality in cross-sectional survey research,” *Accounting, Organizations and Society*, vol. 39, no. 7, 2014, doi: 10.1016/j.aos.2013.12.001.

[28] S. L. Zulu, M. Chabala, and E. Zulu, “Perceptions and beliefs influencing intention to use solar energy solutions in Zambian households,” *Built Environment Project and Asset Management*, vol. 11, no. 5, 2021, doi: 10.1108/BEPAM-01-2021-0010.

مركز الأكاديمية للنشر

ACADEMY Publishing Center

RESD

Renewable Energy and Sustainable Development Journal

ISSN 2356-8569